# Nonlinear optical effects in epsilon-near-zero media

*Orad Reshef*[1]*, *Israel De Leon*[2], *M. Zahirul Alam*[1] and *Robert W. Boyd*[1,3]*

Abstract | Efficient nonlinear optical interactions are essential for many applications in modern photonics. However, they typically require intense laser sources and long interaction lengths, requirements that often render nonlinear optics incompatible with new nanophotonic architectures in integrated optics and metasurface devices. Obtaining materials with stronger nonlinear properties is a crucial step towards applications that require lower powers and smaller footprints. Recently, a new class of materials with a vanishing permittivity, known as epsilon-near-zero (ENZ) materials, has been reported to exhibit unprecedented ultrafast nonlinear efficiencies within sub-wavelength propagation lengths. In this Review, we survey the work that has been performed on ENZ materials and the related near-zero-index materials, focusing on the observation of various nonlinear phenomena (such as intensity-dependent refraction, four-wave mixing and harmonic generation), the identification of unique field-enhancement mechanisms and the study of non-equilibrium dynamics. Degenerately doped semiconductors (such as tin-doped indium oxide and aluminium-doped zinc oxide) are particularly promising candidates for ENZ-enhanced nonlinear optical applications. We conclude by pointing towards possible future research directions, such as the search for ENZ materials with low optical losses and the elucidation of the mechanisms underlying nonlinear enhancements.

Nonlinear optical phenomena enable a broad range of applications[1], including telecommunications and all-optical data processing and storage[2,3], spectroscopy[4] and quantum information technologies[5,6]. However, most materials exhibit only an extremely weak optical nonlinearity, even under intense coherent illumination[7]. Consequently, long interaction lengths are needed for the build-up of nonlinear optical phenomena, and these interaction paths are usually obtained by using bulky material structures that are difficult to scale up and to integrate into nanophotonics systems. As a result, a long-standing goal in the field of nonlinear optics has been the development of materials with very large nonlinear responses, whose optical properties can be dramatically changed with a low-power optical field. In addition, it is highly desirable that these materials possess a sub-picosecond time response and are suitable for nanoscale integration through existing complementary metal-oxide–semiconductor (CMOS) fabrication technologies[8].

Recently, it has been established that materials with a vanishingly small permittivity can enable efficient nonlinear optical phenomena[9–14]. These materials are commonly known as epsilon-near-zero (ENZ) materials, and they display a wealth of exotic properties[15–20]. There is also much interest in the intimately related near-zero-index (NZI) metamaterials[21–24]. Research on these topics was pioneered in a series of theoretical papers published at the beginning of the decade on metamaterials with a zero-permittivity wavelength (a wavelength at which the real part of the permittivity vanishes), which predicted substantial enhancements to the electric field in the material, and high conversion efficiencies for harmonic generation[25–30]. Current interest is motivated by the observation that degenerate semiconductors (semiconductors with such a high level of doping that they start showing metallic behaviour) such as tin-doped indium oxide (ITO) and aluminium-doped zinc oxide (AZO), which both possess a zero-permittivity wavelength in the near-IR (NIR) range, exhibit a huge enhancement of the nonlinear optical response associated with the ENZ spectral region[10–13]. Some works reported record values for the nonlinear refractive index, several orders of magnitude larger than that of arsenic triselenide glass, which has the largest nonlinear coefficient previously reported[31–33], and an ultrafast (sub-picosecond) response. Moreover, a light-induced change in refractive index as large as 0.7 was reported for ITO[12]. Such a change is unprecedentedly large and thus renders these materials promising for new applications in photonics[9], particularly for systems with limited interaction lengths such as nonlinear

[1]*Department of Physics, University of Ottawa, Ottawa, Ontario, Canada.*

[2]*School of Engineering and Sciences, Tecnologico de Monterrey, Monterrey, Nuevo Leon, Mexico.*

[3]*Institute of Optics and Department of Physics and Astronomy, University of Rochester, Rochester, NY, USA.*

**e-mail: orad@reshef.ca; boydrw@mac.com*

https://doi.org/10.1038/s41578-019-0120-5

Table 1 | **Third-order nonlinear optical coefficients of selected materials and metamaterials**

| Material | $\chi^{(3)}$ $(m V^{-1})^2$ | $n_2$ $(m^2 W^{-1})$ | $\lambda_{probe}$ (nm) | Pulse width | Comments |
|---|---|---|---|---|---|
| ***Metals*** | | | | | |
| Silver[171,172] | $3.4\times10^{-17}$ | – | 396 | 28 ps | DFWM |
| Silver[7,173] | $2.8\times10^{-19}$ | – | 1060 | ps | THG |
| Gold[7,171,172] | $2.1\times10^{-16}$ | $2.6\times10^{-14}$ | 532 | 28 ps | DFWM |
| Gold[7,174] | $(-1.4+5i)\times10^{-16}$ | – | 532 | 30 ps | *z*-scan |
| Gold[175] | $(4.67+3.03i)\times10^{-19}$ | – | 796 | 100 fs | Kretschmann–Raether configuration |
| Gold[7,173] | $7.6\times10^{-19}$ | – | 1,060 | ps | THG |
| ***Transparent conducting oxides*** | | | | | |
| AZO[52] | $3.5\times10^{-19}$ | $5.2\times10^{-16}$ | 1,311 | 100 fs | ITM |
| AZO[13] | $(4+1i)\times10^{-20}$ | $3.5\times10^{-17}$ | 1,310 | 100 fs | XPM |
| ITO[55] | $5.6\times10^{-20}$ | $4.1\times10^{-18}$ | 720 | 200 fs | *z*-scan; $\lambda_{ZE}$ unreported |
| ITO[12] | – | $6\times10^{-18}$ | 970 | 150 fs | *z*-scan; $\lambda_{ZE}=1240$ nm |
| ITO[12] | – | $2.6\times10^{-16}$ | 1,240 | 150 fs | *z*-scan; $\theta=0°$ |
| ITO[12,48] | $(1.60+0.50i)\times10^{-18}$ | $1.1\times10^{-14}$ | 1,240 | 150 fs | *z*-scan; ITM; $\theta=60°$ |
| ITO[11] | $3.5\times10^{-18}$ | – | 1,550 | 150 fs | THG |
| ITO[10] | $3\times10^{-21}$ | – | 1,400 | 50 fs | THG |
| ITO[176] | $10^{-21}$ | – | 1,900 | 5.5 ns | THG; $\lambda_{ZE}$ unreported |
| ***Metamaterials*** | | | | | |
| Gold nano-antennas[128] on ITO | – | $-3.7\times10^{-13}$ | 1,420 | 100 fs | *z*-scan |
| ENZ metamaterial[135] (gold nanorods) | – | $-2.4\times10^{-15}$ | 600 | 50 fs | *z*-scan, $\theta=60°$ |
| ENZ metamaterial[60] (Ag–$SiO_2$ thin film stack) | $\sim10^{-19}$ | – | 820, 885 | 100 fs | ITM |
| ***Organic materials*** | | | | | |
| TDBC[61] | $1.2\times10^{-16}$ | $1.7\times10^{-14}$ | 500 | 100 fs | *z*-scan; $\theta=45°$ |
| HTJSq[61] | $7\times10^{-18}$ | $3.5\times10^{-15}$ | 565 | 100 fs | *z*-scan; $\theta=0°$ |

Unless otherwise stated, the pump wavelength is set to $\lambda_{ZE}$. All measurements were performed using p-polarized excitation. $\chi^{(3)}$, third-order susceptibility; $\lambda_{probe}$, wavelength of probe beam; $\theta$, incidence angle of pump beam; AZO, aluminium-doped zinc oxide; DFWM, degenerate four-wave mixing; HTJSq, [2,4-bis[8-hydroxy-1,1,7,7-tetramethyljulolidin-9-yl] squaraine]; ITM, inverse transfer matrix; ITO, indium tin oxide; $n_2$, nonlinear refractive index; TBDC, sodium [5,6-dichloro-2-[[5,6-dichloro-1-ethyl-3-(4-sulphobutyl)-benzimidazol-2-ylidene]-propenyl]-1-ethyl-3-(4-sulphobutyl)-benzimidazolium hydroxide]; THG, third-harmonic generation; XPM, cross-phase modulation. Information on the z-scan method can be found in REFS[177,178].

photonic metasurfaces[34]. Furthermore, numerous fundamental studies have been reported that demonstrate ENZ-enhancement of other nonlinear optical processes, such as harmonic generation[10,11,35], wave mixing and frequency conversion[13,36,37] and electro-optical effects[38–40]. Nonlinear optical coefficients of several ENZ materials are listed in TABLE 1. Efficient practical devices such as all-optical and electro-optical modulators have also been proposed that exploit such enhanced nonlinear effects[41–43].

In this Review, we survey ENZ and NZI materials, comparing their optical properties and summarizing their practical implementations. We describe the theoretical understanding of the origin of the huge nonlinear response of ENZ materials, including field-enhancement mechanisms unique to this class of materials. We then turn to the primary focus of this article and review the experiments that have explored the relation between ENZ behaviour and nonlinear optical response. We conclude with a discussion on the future of this nascent field.

## Background

ENZ materials exhibit a vanishing real part of the permittivity at a spectral point known as the zero-permittivity wavelength, $\lambda_{ZE}$; however, the permeability $\mu$ remains finite and non-zero. By contrast, in NZI materials the real part of the refractive index $n$ (or the effective refractive index $n_{eff}$ in the case of a metamaterial) vanishes at the zero-index wavelength, $\lambda_{ZI}$. When the real part of both the permittivity and the permeability simultaneously equal zero, NZI materials are also often called epsilon-and-mu-near-zero, double-zero or zero-index materials[22,24,44].

We remark that both the dielectric permittivity $\epsilon$ and the refractive index $n\equiv\sqrt{\epsilon\mu}$ are complex quantities. Thus, even when the real part of $\epsilon$ vanishes, its imaginary part usually remains non-zero, and thus both the

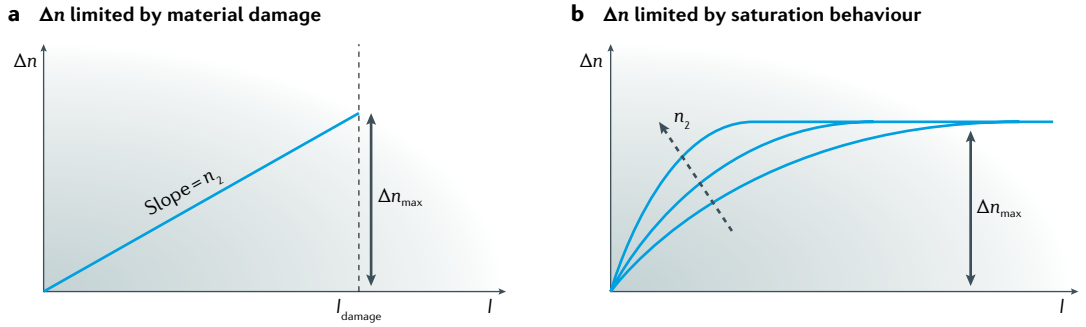


Fig. 1 | **Maximum changes in refractive index. a** | Change in the refractive index, $\Delta n$, as a function of the applied optical field intensity $I$ when changes to $n$ are limited by the damage threshold of the material. $n_2$ is the nonlinear refractive index. **b** | $\Delta n$ as a function of $I$ in the case in which $n$ is limited by the saturation behaviour of the material. The dashed arrow indicates the effect of field-enhancement mechanisms, which increase the slope but do not increase the maximum value of $\Delta n$, $\Delta n_{max}$.

real and imaginary parts of $n$ are also non-vanishing. The contribution of the imaginary permittivity to the refractive index can be significant in many materials. Assuming no magnetic responses (that is, $\mu \to 1$), at the zero-permittivity wavelength the real part of the refractive index is given by:

$$n' = \sqrt{\frac{|\epsilon''|}{2}} \quad (1)$$

where the single and double primes denote the real and imaginary parts, respectively. For ITO, which has a zero-permittivity wavelength in the NIR, the imaginary part of the permittivity ($\epsilon'' \approx 0.3$) yields a small real value of the refractive index of around 0.4 (REFS[12,45]). Therefore, although it might appear that the refractive index must vanish along with a vanishing permittivity, a distinction must be maintained between ENZ and NZI materials.

## Mechanisms for large nonlinearity

Before discussing experimental results, we survey the different physical microscopic processes and unique field enhancement mechanisms that have been discovered in ENZ and NZI materials.

When discussing strong Kerr-like optical nonlinearities, in which changes in the refractive index usually scale linearly with the nonlinear refractive index $n_2$ and the intensity $I$ as $\Delta n = n_2 I$, typically one searches for a material with a large $n_2$ (REF.[7]):

$$n_2 = \frac{3\chi^{(3)}(\omega;\omega,\omega,-\omega)}{4n_0 \mathrm{Re}(n_0)\epsilon_0 c} \quad (2)$$

where $\chi^{(3)}$ is the third-order susceptibility, $n_0$ the linear refractive index, $\epsilon_0$ the vacuum permittivity and $c$ the speed of light. Alternatively, one could look to maximize a given material figure of merit (see, for example, REFS[46,47]). However, the maximum nonlinear phase shift that can be obtained in a material with a given $n_2$ is often limited by the damage threshold or saturation behaviour of the material (FIG. 1). In some sense, what is truly required for many nonlinear applications is a considerable total change in the refractive index $\Delta n$; the nonlinear refractive index $n_2$, which may be increased for a particular material using suitable field-enhancement mechanisms, describes only the slope of this change with respect to the applied optical field intensity $I$. In a material with a large damage threshold and pronounced saturation effects, increased values of $n_2$ merely enable the achievement of the maximum value of $\Delta n$ at smaller intensities (FIG. 1b).

### *Apparent divergence of $n_2$*

Within the context of bound electron nonlinearities, a conceptually intriguing consequence of a vanishing refractive index is the seeming divergence of the nonlinear refractive index $n_2$, because a factor of $\mathrm{Re}(n_0)$ appears in its denominator (Eq. 2). However, a necessary assumption underlying this equation (that is, that $|n_2 I / n_0| \ll 1$) is violated when $n_0$ is small[48]. Therefore, Eq. 2 is not suitable for describing nonlinear refraction in low-index media, and the divergent behaviour of $n_2$ is merely an artefact of its derivation. In these systems, the intensity-dependent index of refraction should be calculated directly from the susceptibility:

$$n(I) = \sqrt{\epsilon(\mathbf{E})} = \sqrt{\epsilon^{(1)} + 3\chi^{(3)}|\mathbf{E}|^2} \quad (3)$$

where $\epsilon^{(1)}$ is the complex linear permittivity and $|\mathbf{E}|$ the magnitude of the electric field within the material. The third-order susceptibility $\chi^{(3)}$ and the total index change $\Delta n$ should therefore be considered as the relevant metrics in assessing the intensity-dependent refractive index of ENZ media. In this case, $\Delta n$ is the difference between the refractive index at high intensity and at low intensity, and is not necessarily equal to $n_2 I$. However, because $n_2$ remains the most frequently reported figure of merit for nonlinear refraction, we quote those values in the rest of the text. Here, we interpret $n_2$ to be the value of the initial slope of the refractive index with respect to incident intensity ($n_2 = \frac{\mathrm{d}n}{\mathrm{d}I}|_{I=0}$), where $n_2 I$ is smallest and the inequality $\frac{n_2 I}{n_0} \ll 1$ is perhaps not violated.

The question arises of what is the true origin of the large nonlinearities that have been reported in ENZ media if the diverging $n_2$ is merely a numerical artefact. Whereas $n_2$ is a quantity that must be inferred from laboratory measurements and so could perhaps be open to misinterpretation, changes in reflectivity $\Delta R$, changes in

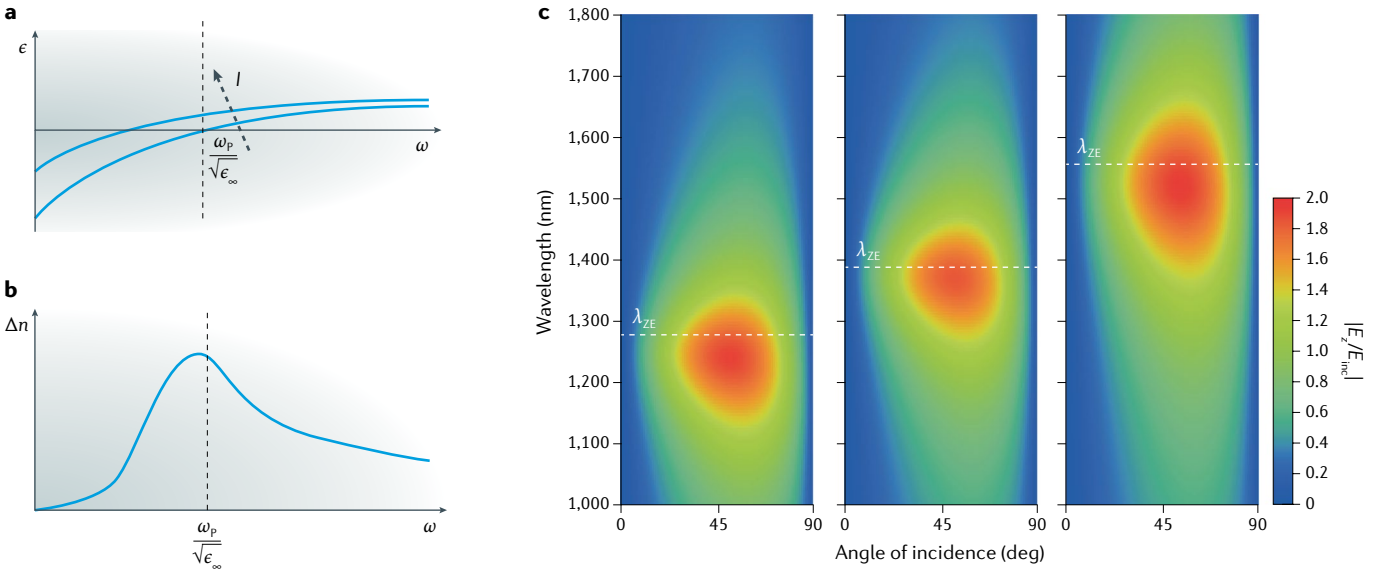


Fig. 2 | **Mechanisms underlying nonlinearity and enhancement. a** | Under intense laser excitation, the plasma frequency $\omega_P$ is modified as a function of pump intensity $I$, displacing the permittivity dispersion function $\epsilon(\omega)$. **b** | This shift in plasma frequency leads to a change in refractive index $\Delta n$, which is largest at the zero-permittivity wavelength, $\lambda_{ZE}$. $\epsilon_\infty$ is the permittivity at high frequency. **c** | Enhancement of the electric field **E** at the air/indium tin oxide (ITO) interface in a 37-nm-thick ITO film as a function of wavelength and angle of incidence for p-polarized light. The maximum field enhancements occur at each film's respective $\lambda_{ZE}$ and around an incident angle $\theta = 45°$. Here, $\lambda_{ZE} = 1{,}270$ nm (left), 1,390 nm (centre) and 1,550 nm (right). $E_z$ is the component of the electric field normal to the interface inside of ITO, $E_{inc}$ is the incident field. Adapted with permission from REF.[11], Optical Society of America.

refractive index $\Delta n$ and any associated phase changes $\Delta\varphi$ are all laboratory-observable quantities, which together hint at verifiable large nonlinear effects. Eq. 3 thus tells us that there must be some enhancement in $\chi^{(3)}$, in $|E|$, or in both quantities. In a later section, we examine the behaviour of these two terms in ENZ media in closer detail.

### *Plasma frequency shift*

Metals and degenerately doped semiconductors feature a permittivity dispersion profile based on free electrons described by the Drude model[49]:

$$\epsilon(\omega) = \epsilon_\infty - \frac{\omega_P^2}{\omega^2 + i\gamma\omega} \tag{4}$$

where $\epsilon_\infty$ is the high-frequency permittivity, $\gamma$ the electron damping term and $\omega_P$ the plasma frequency, given by:

$$\omega_P \equiv \sqrt{\frac{Ne^2}{m_e^* \epsilon_0}} \tag{5}$$

with $N$ the free-electron volume density and $m_e^*$ the effective mass of the electron.

Upon intense laser excitation, several physical mechanisms may temporarily modify the plasma frequency, which reshapes the material dispersion throughout the nearby spectrum (FIG. 2a,b). This reshaping typically depends on the pulse duration and operating wavelength. An optical pump illuminating the material with photon energy larger than the bandgap may increase the carrier density in the conduction band. As described by Eq. 5, an increase in carrier density leads to an increased plasma frequency, and thus results in a reduction of the real part of the permittivity[9,36]. In a doped semiconductor, the photon energy needs to be larger than the bandgap energy (for example, 2.5 eV for AZO[9]); in a metal it needs to be larger than the interband transition energy (for example, 1.8 eV for gold[50]). If an optical pump with smaller photon energy is applied, electron heating may cause a redistribution of electrons within the conduction band. This effect, together with the non-parabolicity of the conduction band in certain materials, leads to an increase in $m_e^*$ in Eq. 5, and hence to a redshift of the plasma frequency[51]. If the pump frequency coincides with the plasma frequency (at the zero-permittivity wavelength), the free electrons in the material are excited resonantly and this effect becomes most pronounced[12,52]. A plasma frequency shift can also be initiated by locally increasing the carrier density using a static voltage[38] or by tuning the effective electron mass using thermal control[53]; however, thermal processes are known to be slow, and electronic gating affects only a small region of material (only a 5-nm-thick accumulation layer)[38,39,53,54]. The dependence of the nonlinear response on the carrier concentration has been investigated for ITO, albeit not in the ENZ regime[55].

Two material properties result in plasma-frequency-related effects being more marked in degenerately doped semiconductors than in noble metals. First, they have a free-electron density that may be two orders of magnitude smaller than that of noble metals, which results in a much smaller electron heat capacity and larger changes in the electron temperature[12,38]. Second, owing to the non-parabolicity of the conduction band[14,53,56,57],

the effective mass, and therefore the plasma frequency, is more dependent on the electron temperature.

Recently, it was shown that nonlocal phenomena (such as spatial dispersion) play an important role in determining the linear optical response of ENZ nanofilms made of CdO (REF.[58]). We stress that such nonlocal effects are not captured in Eq. 4, and that more work is required to understand the implications of nonlocal effects for the nonlinear refractive index of ENZ materials based on conductive oxides.

## Enhancement mechanisms

We mentioned that the large nonlinear optical response of ENZ materials is associated with enhancements in their nonlinear susceptibility and/or in the electric field that occurs within the material owing to the low material permittivity. Here, we comment on various enhancement mechanisms that have been reported. As of this writing, it is not yet clear which mechanisms are dominant in which contexts and in which materials.

### *Third-order susceptibility*

A form of Eq. 3 that includes higher-order susceptibilities has been used to extract a value of $\chi^{(3)}$ for ITO near its zero-permittivity wavelength, $\chi^{(3)} = 1.60 + 0.50i \times 10^{-18}\,\mathrm{m^2\,V^{-2}}$ (REF.[48]) Similarly, the $\chi^{(3)}$ of AZO was estimated to be $3.5 \times 10^{-19}\,\mathrm{m^2\,V^{-2}}$ at the zero-permittivity wavelength[52]. These values are of comparable order to the third-order susceptibility of crystalline silicon ($\chi^{(3)} = \mathcal{O}[10^{-19}]\,\mathrm{m^2\,V^{-2}}$; REF.[59]); therefore, they alone cannot account for any significant nonlinear phase shifts within sub-wavelength interaction regions. In measurements in which $\chi^{(3)}$ has been resolved as a function of wavelength[13,52,60,61], it is sometimes observed to be larger in a narrow region surrounding the zero-permittivity wavelength[52]; however, the reported values remain within the same order and so cannot really account for the magnitude of the increase in the nonlinear optical response observed when comparing the properties at the zero-permittivity wavelength with those away from it. Indeed, it was explicitly mentioned in REF.[62] that $\chi^{(3)}$ is increased only by a factor of 4 in the ENZ regime, yet the nonlinear conversion efficiency associated with this nonlinearity is enhanced by a factor of 100. We conclude that any enhancements to the third-order susceptibility are negligible in comparison to the overall nonlinear response at the zero-permittivity wavelength. We therefore expect a field-enhancement mechanism intrinsic to ENZ materials that may greatly increase $|\mathbf{E}|$ for a given incident pump field intensity. However, further studies that explicitly examine $\chi^{(3)}$ (rather than $n_2$) over a broad spectral range are needed to properly determine the origin and magnitude of this enhancement mechanism.

### *Continuity of the electric field*

The small magnitude of the permittivity in the ENZ region gives rise to a unique field-enhancement mechanism[28,63]. In the absence of a surface charge, the interface conditions ensure the continuity of the normal component of the electric displacement field. Thus, the magnitude of the normal component of the electric field $\mathbf{E}$ within a medium is proportional to the external field $\mathbf{E}_0$ and to the inverse of its permittivity (that is, $|\mathbf{E}_\perp| \propto \epsilon^{-1}|\mathbf{E}_{0,\perp}|$). For a p-polarized beam incident from air at a given angle of incidence $\theta$, this relation leads to the following expression for the total field within a medium of permittivity $\epsilon$:

$$|\mathbf{E}| = |\mathbf{E}_0| \sqrt{\cos^2\theta + \frac{\sin^2\theta}{\epsilon}} \tag{6}$$

Therefore, at an oblique angle, the electric field within an ENZ medium can be much larger than the incident field (FIG. 2c). This enhancement mechanism results in the pronounced angular dependence observed for many nonlinear effects.

This mechanism is predicted to be further improved in thin films that have a real permittivity tensor with a vanishing out-of-plane component, sometimes called longitudinal ENZ films[28,64,65]. In these materials, the field enhancement is larger, occurs for a wider range of incident angles and is less sensitive to material losses than in an isotropic film with comparable optical constants.

### *ENZ modes and Berreman modes*

An ENZ thin film supports a unique set of propagating eigenmodes, including an unbounded Brewster or Berreman mode[66–70], and in some cases a confined mode known as an ENZ mode[71]. The latter features a flat dispersion profile and a considerable field enhancement enabled by boundary conditions (FIG. 3), as described in the previous subsection. Notably, a film needs to be ultrathin (less than about $\lambda/50$) to support an ENZ mode; for example, an ITO film needs to be at most 25 nm thick to support such a mode. Otherwise, the ENZ mode degenerates into a long-range surface plasmon polariton[72]. Like other confined modes, the ENZ mode is not easily accessed from free space without an extrinsic coupling mechanism.

### *Slow light nonlinear enhancement*

For an unbounded ENZ medium, the group velocity can be shown to be $v_g = \sqrt{\epsilon}\,c$ (REFS[73,74]). Thus, a lossless ENZ medium will feature an asymptotically vanishing group velocity as $\epsilon \to 0$. Indeed, the ENZ mode in FIG. 3a also depicts a vanishing group velocity[70,71]. The fact that slow light propagation has previously been associated with nonlinear enhancements (specifically in regard to structural slow light[75–77]) has led some researchers to make a connection between ENZ-based nonlinearities and slow light effects[20,23,78–80]. As yet, no experiments have been performed that explicitly extract the contribution of slow light propagation to the nonlinear optical response of ENZ materials, so this connection remains open to debate.

## Materials

A discussion of the properties of low-index materials stimulates the question of what materials may possess them. In this section, we review attempts to identify and fabricate homogeneous ENZ materials, to develop ENZ and NZI metamaterials, and to incorporate ENZ materials in devices for various applications.

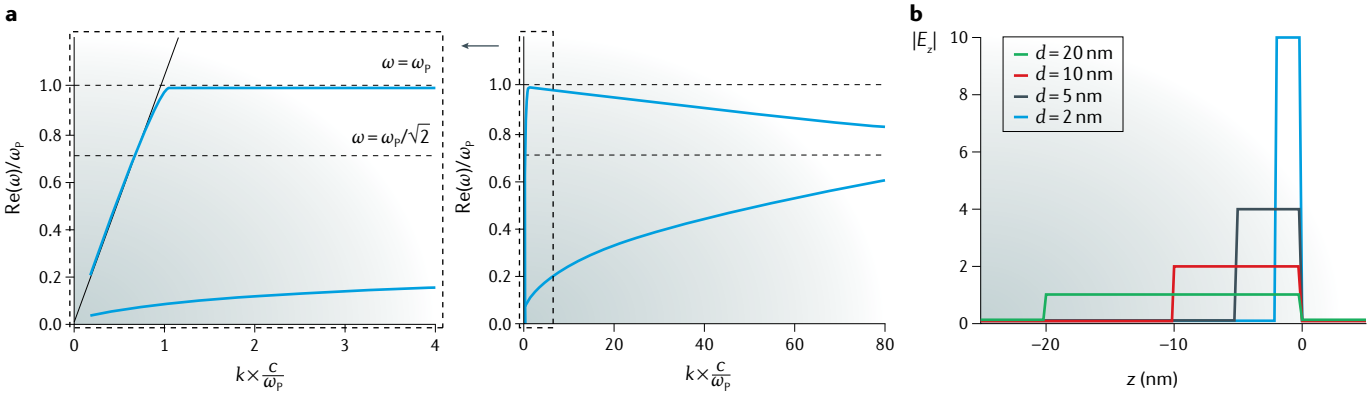


Fig. 3 | **Field enhancement in the epsilon-near-zero mode. a** | For a film thickness much smaller than the skin depth (the penetration depth of electromagnetic radiation in the material), a mode with a flat dispersion, known as the epsilon-near-zero (ENZ) mode, appears at $\mathrm{Re}(\omega) = \omega_P$. $\omega_P$, plasma frequency; $k$, wavenumber in the direction parallel to the surface; $c$, speed of light. **b** | Magnitude of the component of the electric field normal to the interface $|E_z|$ as a function of $z$ for various slab thicknesses. A larger field is generated within thinner films. $|E_z|$ is normalized to its value for a thickness $d = 20$ nm. Adapted with permission from REF.[71], AAAS.

### *Naturally occurring ENZ materials*

Although at first glance a permittivity equal to zero might seem exotic, naturally occurring materials routinely exhibit ENZ regimes near strong optical resonances, such as the bulk plasma resonance and phonon resonances. Therefore, all metals have a permittivity zero crossing at the bulk plasma resonance, which occurs at the plasma frequency (typically in the UV band)[81–83]. Recently, there has been increased interest in degenerately doped semiconductors, such as ITO, AZO and gallium-doped zinc oxide (GZO)[45,84–95]. These materials may all feature a plasma frequency in the NIR band. This property has made them very useful for demonstrations of optical nonlinearity, owing to the accessibility of intense pulsed laser sources in the NIR spectral range and the proximity of their zero-permittivity wavelengths to telecommunications wavelengths, around 1,550 nm. The plasma frequency can be tuned as a function of deposition parameters[86] (FIG. 4a), carrier dopant concentration[38,54] (FIG. 4b) or post-deposition annealing[11,89]. Much work has been done in engineering the zero-permittivity wavelength to a wide range of wavelengths[86–89]. In addition, because they are both transparent and conductive, these materials are already being widely used by commercial vendors for solar applications and touchscreen display technologies; therefore, their industrial manufacturing procedures are mature, although perhaps not optimized for optical properties. Finally, correlated metals, such as $SrVO_3$ and $CaVO_3$, have been identified as promising alternatives to transparent conducting oxides[96].

In the visible regime, transition metal nitrides such as titanium nitride and zirconium nitride have been used[35,86,97]. Organic materials, which have the benefit of reduced damping loss, have been shown to have a zero-permittivity wavelength tunable within the visible regime[61,98,99]. In the mid-IR (MIR), indium-doped and dysprosium-doped cadmium oxide behave as ENZ materials with high electron mobilities[14,100]. Silicon carbide[95,101,102] and fused silica[103,104] are also widely known to possess zero-permittivity wavelengths in the MIR due to phononic resonances. Finally, topological insulators (for example $Bi_{1.5}Sb_{0.5}Te_{1.8}Se_{1.2}$) may support ENZ conditions in the UV and visible ranges[105]. These materials and others, such as titanium oxynitride, can be deposited in such a manner that they exhibit multiple zero-permittivity wavelengths, although typically at the cost of a considerable imaginary part of the permittivity[106].

### *Metamaterials*

ENZ and NZI optical responses can both be engineered in metamaterials[24]. The permittivity can be tuned using nanoparticle resonances, which makes the ENZ condition itself relatively trivial to achieve in a composite material[107]. A typical configuration with a straightforward fabrication process is a metal–dielectric stack[60,108–113] (FIG. 4c): at optical frequencies, dielectric materials possess positive permittivities and metals possess negative ones, so it can be intuitively understood that a composite of these two material classes may have some weighted average that can approach zero[112]. The resulting effective permittivity is anisotropic, and in the long-wavelength limit equals[112,113]:

$$\epsilon_\perp = \frac{d_m \epsilon_m + d_d \epsilon_d}{d_m + d_d} \qquad \frac{1}{\epsilon_\parallel} = \frac{d_m/\epsilon_m + d_d/\epsilon_d}{d_m + d_d} \tag{7}$$

for the components perpendicular and parallel to the plane, respectively. $d_m$ and $\epsilon_m$ represent the thickness and permittivity of the metal layer, and $d_d$ and $\epsilon_d$ the thickness and permittivity of the dielectric layer, respectively. Metal–dielectric stacks can even be designed to exhibit multiple simultaneous ENZ regimes at nearby wavelengths[114].

By contrast, a refractive index equal to zero is much more challenging to engineer. In particular, at optical frequencies, the permeability is fixed to $\mu = 1$ owing to the lack of atomic magnetic response. Artificial magnetic resonances were first introduced using sub-wavelength plasmonic split-ring resonators[115], and the magnetic responses were paired with dipole resonances to form

the basis of the first negative-index and zero-index metamaterials, culminating in the 'fishnet' structure[116,117] (FIG. 4d). Following this work, Mie resonances in dielectric nanoparticles were exploited to achieve lossless magnetic responses[118,119]. Although these particles must be necessarily larger than plasmonic particles to exhibit comparable resonance wavelengths, they have no resistive losses and therefore have potential for improved optical performance[120,121]. Mie resonances were used to achieve all-dielectric zero-index metamaterials[122,123], which were ultimately extended to a silicon photonic platform[44,124–126] (FIG. 4e).

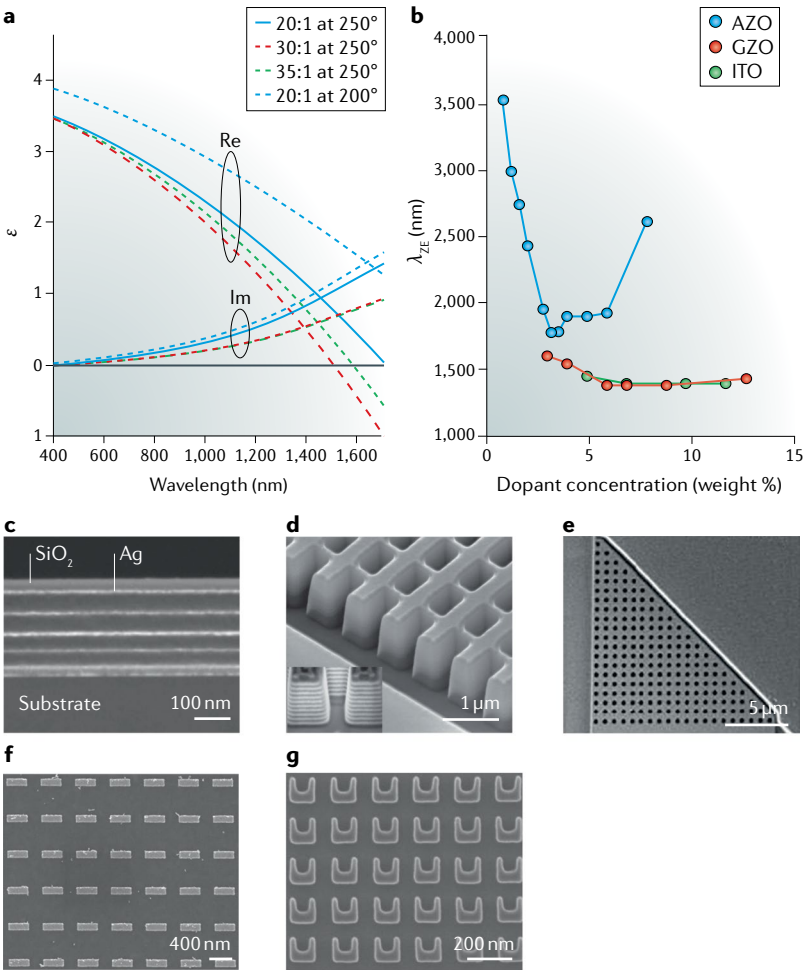


Fig. 4 | **Epsilon-near-zero and near-zero-index materials. a** | The permittivity of aluminium-doped zinc oxide (AZO) as a function of wavelength for different deposition parameters, displaying Drude dispersion and demonstrating the wide tunability of the zero-permittivity wavelength. **b** | The zero-permittivity wavelength for AZO, gallium-doped zinc oxide (GZO) and indium tin oxide (ITO) as a function of dopant concentration. **c** | An epsilon-near-zero (ENZ) metamaterial consisting of an Ag–$SiO_2$ metal–dielectric thin film stack. **d** | A 'fishnet' zero-index metamaterial formed of silver and magnesium fluoride. **e** | An all-silicon Dirac-cone zero-index metamaterial. **f** | Gold nano-antennas on ITO for enhanced coupling and nonlinearity. **g** | U-shaped antennas formed of titanium nitride that also enable plasmonic resonances at visible wavelengths. Panel **a** is adapted with permission from REF.[94], IOP Publishing. Panel **b** is adapted with permission from REF.[86], Optical Society of America. Panel **c** adapted from REF.[60], CC-BY-4.0. Panel **d** adapted from REF.[116], Springer Nature Limited. Panel **e** is adapted with permission from REF.[124], Optical Society of America. Panel **f** adapted from REF.[128], Springer Nature Limited. Panel **g** is adapted with permission from REF.[97], AAAS.

### *Materials with ENZ inclusions*

The final class of ENZ platforms that is relevant to our discussion is that of nanostructures or metamaterials that include a natural ENZ material in their design. These structures either aim to enhance the nonlinearity of a given device with the help of an ENZ material, or try to eliminate inherent obstacles associated with ENZ materials (such as impedance mismatch[127–129]). Examples include coupling ENZ layers to nano-antennas[53,127,128] (FIG. 4f) or structuring the ENZ materials themselves into nano-antennas[51,57,97,130] (FIG. 4g) to enable nanoparticle resonances at wavelengths other than $\lambda_{ZE}$. Often an ultrathin ENZ film (≤20 nm in thickness) is incorporated in a device as the active medium[39,131,132]. Finally, a class of single-inclusion metamaterials using ENZ materials as a background medium, known as photonically doped materials, was developed[133]. When a dielectric component, known here as the dopant, is embedded within an ENZ host, the permeability of the entire structure (and therefore its refractive index and impedance) can be freely tuned while the permittivity remains fixed. These metamaterials were demonstrated in the microwave regime using metallic waveguides operating at cut-off[133].

## Experimental studies

ITO, AZO and related material platforms have been the subject of extensive experimental studies. Here, we review experiments that have been performed to measure phenomena such as nonlinear refraction, harmonic generation and wave mixing using ultrafast optical pulses. We also discuss the materials' behaviour in the presence of a static field, as well as other nonlinear phenomena demonstrated using these platforms.

### *Intensity-dependent index of refraction*

***Degenerate case.*** A large intensity-dependent index of refraction ($n_2 = 2.6 \times 10^{-16}\,m^2\,W^{-1}$) was observed in a 310-nm-thick ITO film at its zero-permittivity wavelength, using 150 fs pulses in a *z*-scan measurement[12]. This value was reported to be over 40 times as large as the value measured away from the ENZ region for normal-incidence illumination, and increased by more than an additional factor of 40 when the sample was excited using a p-polarized beam at oblique incidence, peaking at a value of $1.1 \times 10^{-14}\,m^2\,W^{-1}$ for an incidence angle of 60° (FIG. 5a). Moreover, the total change in refractive index $\Delta n$ saturated at a value of 0.72 (FIG. 5b, top). A pump–probe experiment indicated a non-instantaneous ultrafast response, with a relaxation time of 360 fs and a rise time estimated to be shorter than the pulse width. More comprehensive modelling of nonlinear refraction in ITO concluded that nonlinear optics enters the non-perturbative regime in ENZ materials[48]. Notably, the contribution to refraction from third-order, fifth-order and even seventh-order effects was found to exceed the contribution from the linear permittivity at the highest probed intensities (FIG. 5b, bottom).

Multiple measurements were also performed on AZO near its zero-permittivity wavelength ($\lambda_{ZE} = 1{,}300$ nm), in which a similarly large nonlinear refractive index was reported ($n_2 = 5.17 \times 10^{-16}\,m^2\,W^{-1}$)[52]. This value was found to be over 35 times as large as the value measured away

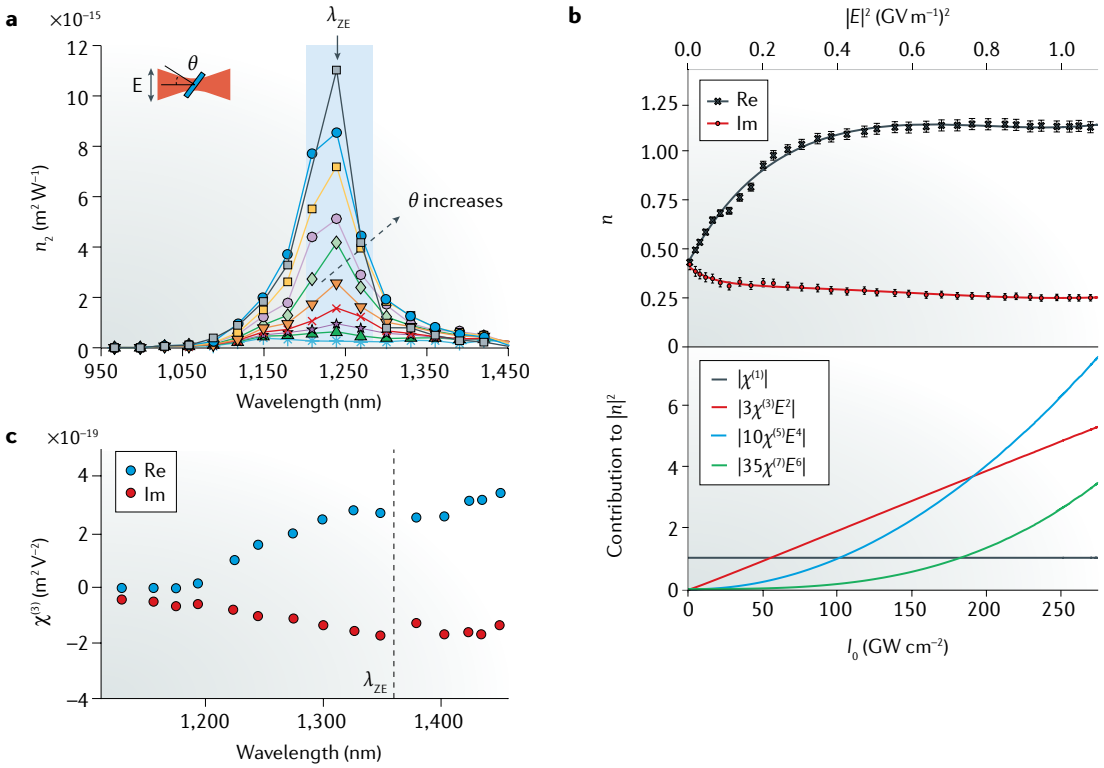


Fig. 5 | **Intensity-dependent refraction in indium tin oxide. a** | Wavelength dependence of the nonlinear refractive index $n_2$ of indium tin oxide (ITO) near its zero-permittivity wavelength $\lambda_{ZE} = 1{,}240$ nm. The nonlinear response is enhanced in the epsilon-near-zero (ENZ) region of the spectrum (shaded) and is stronger for higher incidence angles $\theta$ of the electric field **E**. **b** | The total refractive index $n$ experiences saturation behaviour at high intensities, with a total change of index $\Delta n_{max} = 0.72$. The solid lines represent a fit with the addition of complex $\chi^{(5)}$ and $\chi^{(7)}$ terms (top). The error bars correspond to the error of the measurement. Absolute contribution of the various orders of the nonlinear susceptibility to the refractive index at the zero-permittivity wavelength (bottom). **c** | Wavelength dependence of the third-order susceptibility $\chi^{(3)}$ for aluminium-doped zinc oxide (AZO), which exhibits a small increase at $\lambda = 1{,}330$ nm, near the zero-permittivity wavelength $\lambda_{ZE} = 1{,}360$ nm. Panel **a** is adapted with permission from REF.[12], AAAS. Panel **b** is adapted with permission from REF.[48], Optical Society of America. Panel **c** is adapted from REF.[52], CC-BY-4.0.

from the zero-permittivity wavelength ($\lambda = 1{,}400$ nm.) A moderate increase in $\chi^{(3)}$ when compared with the non-ENZ regime was also reported, with the real part reaching a peak value of $2.8 \times 10^{-19}$ m$^2$ V$^{-2}$ at a wavelength of 1,330 nm (FIG. 5c). Here, a probe pulse was used to measure the transmission and reflection coefficients for a stationary 900-nm-thick film under degenerate pump laser excitation, and the inverse transfer matrix method was used to extract the optical constants.

A large intensity-dependent index of refraction was also observed in specially prepared organic ENZ thin films[61]. In this work, the authors studied 55-nm-thick films of polymethine dyes. These films were synthesized to feature ENZ regions spanning the visible spectrum, with zero crossings between 500 nm and 570 nm. The authors reported a value of $n_2$ as high as $1.7 \times 10^{-14}$ m$^2$ W$^{-1}$, two orders of magnitude larger than in the non-ENZ range. Unfortunately, these organic materials feature prohibitively low damage thresholds; whereas work with ITO and AZO may use peak operating intensities exceeding 1,000 GW cm$^{-2}$, and in some cases 2,000 GW cm$^{-2}$ (REF.[13]), in this work the intensity was kept below 45 GW cm$^{-2}$ to prevent laser-induced damage[61].

Degenerate nonlinear effects were also studied at the zero-permittivity wavelength of ITO colloidal nanocrystals with diameters of ~8 nm that were fabricated by using wet chemistry[90]. The authors stated that the nonlinearity would be further enhanced by the rich surface trap states. They demonstrated control over the doping concentration, tuning the zero-permittivity wavelength from 1,300 nm to 1,600 nm. Using 35 fs pulses, they observed nonlinear absorption coefficients as large as $-5.14 \times 10^{-10}$ m W$^{-1}$, with a relaxation time of 450 fs. A unique aspect of this work was the use of the material as the saturable absorber in a mode-locked laser, generating a 600 fs pulse train.

Finally, metasurfaces can be used to further enhance nonlinear refraction of an ENZ thin film. Nanoscale gold dipole antennas (360 nm × 110 nm × 30 nm) were fabricated on an ENZ substrate to aid in impedance-matching and field-enhancement[128]. The antennas were engineered to support a localized surface plasmon resonance at the zero-permittivity wavelength of the substrate film ($\lambda_{ZE} = 1{,}420$ nm), providing a 50-fold enhancement of peak intensity. Additionally, the antennas acted as mode converters, efficiently coupling light from free space to the ENZ medium at normal incidence. Together, the film and the antennas combined to form a 50-nm-thick metasurface that exhibited a giant magnitude of nonlinear refraction, $|n_2| = 3.73 \times 10^{-13}$ m$^2$ W$^{-1}$.

The bandwidth of the nonlinearity was also greatly increased to over 400 nm and featured a sign change. Nonlinear absorption also featured a sign change, changing from saturable to reverse saturable absorption at 1,440 nm. The total refractive index change was large, $\Delta n > 2.5$, and the total response time (rise and relaxation) was only 50% longer than that of the bare ITO film. The main limitation of this platform is the damage threshold, which is limited to that of the gold antennas[134].

It is interesting to consider whether $n_2$ could be similarly large for a zero-permittivity or zero-index wavelength arising through structure, as opposed to being an intrinsic material property. To this end, a *z*-scan measurement was performed in an anisotropic ENZ metamaterial composed of high-aspect-ratio (150 nm × 17 nm) gold nanorods with $\lambda_{ZE} = 600$ nm (REF.[135]). The measured maximum nonlinear refraction ($n_2 = -2.4 \times 10^{-15}$ m$^2$ W$^{-1}$) and absorption ($\beta = -1.0 \times 10^{-7}$ m W$^{-1}$) coefficients were 20 and 100 times larger, respectively, than those of a uniform 50-nm-thick gold film. However, we note that other metal–dielectric stacks also exhibit nonlinearities an order of magnitude larger than those of the metals that they incorporate, with no obvious dependence on the effective zero-permittivity wavelength (see, for example, REFS[108,136]). When compared to measurements performed away from $\lambda_{ZE} = 600$ nm (for example at $\lambda = 550$ or 650 nm), the nonlinearity of the ENZ metamaterial in REF.[135] at $\lambda_{ZE}$ does not appear to be substantially larger. However, if the sample is tilted by 60°, the nonlinear coefficients at $\lambda_{ZE}$ greatly exceed those at other wavelengths.

***Non-degenerate case.*** Non-degenerate nonlinear effects (those resulting from an excitation involving multiple distinguishable optical waves such as cross-phase modulation and other four-wave mixing effects) provide a different perspective from which to examine the origins and mechanisms of nonlinearity. Reports include the observation of an intensity-dependent refractive index change performed using oxygen-deprived AZO under ENZ conditions. The authors noted that for the same small change in refractive index, there would be a much larger change in optical wave impedance (and therefore reflectance) for a beam centred at the zero-permittivity wavelength. The sample was excited with photon energies greater than the bandgap to induce interband transitions ($\lambda = 325$ nm) and probed at the zero-permittivity wavelength ($\lambda_{ZE} = 1{,}300$ nm). Relative changes in reflectivity ($\Delta R/R$) and transmissivity ($\Delta T/T$) as large as 40% and 30%, respectively, were reported, with a total rise and relaxation time under 1 ps. Using these values and the inverse transfer matrix method, a maximum change of refractive index of $\Delta n = -0.17$ at a peak pump fluence of 3.6 mJ cm$^{-2}$ was estimated.

Follow-up work directly examined nonlinear refraction in AZO[13]. The authors used a pump beam centred at $\lambda = 785$ nm and swept a cross-polarized probe beam from 1,150 nm to 1,550 nm. They observed a sixfold enhancement of the real part of $n_2$ at the zero-permittivity wavelength compared with values at other nearby wavelengths, although no significant enhancement of $\chi^{(3)}$ was observed. A large change of index $\Delta n = 0.4$ and ratio of $\Delta n/n \approx 4.4$ were also reported. These striking results are in large part due to the small imaginary part of the permittivity that is achievable in this material platform: at the zero-permittivity wavelength, $\mathrm{Im}(n) = 0.09$. However, when compared with the degenerate measurements in AZO, non-degenerate optical excitation was found not to be optimal in fully exploiting the nonlinear properties of AZO (FIG. 6a).

A shift in the probe beam of up to 20 nm dependent on the pump intensity was also observed in AZO. Similar pump–probe experiments in AZO also revealed a wavelength shift of the probe signal of up to 13 nm (REF.[137]) (FIG. 6b). The phenomenon was in part attributed to the temporal dynamics of the induced change in refractive index through cross-phase modulation. These results indicate clearly that the magnitude of the spectral shift is strongly dependent on the probe wavelength. Furthermore, it was observed that the probe can be blueshifted or redshifted depending on the temporal distance between the pump and probe beams. More recent work has extended this wavelength shift to up to 48 nm — that is, twice the pulse bandwidth[37].

A large modulation of the optical properties of AZO was experimentally demonstrated at a wavelength close to the zero-permittivity wavelength ($\lambda_{ZE} = 1{,}300$ nm) with a two-colour (UV and NIR) optical pumping scheme, bringing together all that has been concluded about the different pump mechanisms of AZO[36]. The UV pump ($\lambda_{UV} = 262$ nm) promotes interband transitions and increases the plasma frequency, whereas the NIR pump ($\lambda_{NIR} = 787$ nm) induces hot-electron effects that decrease the plasma frequency. These two processes were combined to perform a thorough investigation of the optical response of a 900-nm-thick AZO film (FIG. 6c). Furthermore, by controlling the temporal delay between the UV and NIR pumps, it is possible to enter a regime in which the temporal response of the combined nonlinear processes is either faster or slower than the response of each individual process. Indeed, the response bandwidth of the AZO film can be increased from 0.8 THz to 2 THz for specific delays between the two pumps, although at the expense of the strength of the overall nonlinear response.

Some preliminary measurements have been performed to examine the non-degenerate nonlinear response of ITO near its zero-permittivity wavelength using the beam-deflection technique[138]. Unlike in *z*-scan, this two-beam method inherently disentangles the effects of nonlinear refraction and nonlinear absorption in the measured signal[139,140]. The authors reported a 5,000-fold enhancement in nonlinear refraction when the probe beam was centred at the zero-permittivity wavelength. Additionally, no polarization dependence was observed, which was interpreted as evidence for the carrier-dependent nature of the nonlinear response.

In a metamaterial study, a pair of silica–silver metal–dielectric stacks with zero-permittivity wavelengths of $\lambda_{ZE} = 820$ nm and 885 nm were characterized[60]. The third-order nonlinearity of the samples at their zero-permittivity wavelengths was found to be of the same order as that of bulk silver ($\chi^{(3)} = 2.8 \times 10^{-19}$ m$^2$ V$^{-2}$). According to this study, this value does not stand out

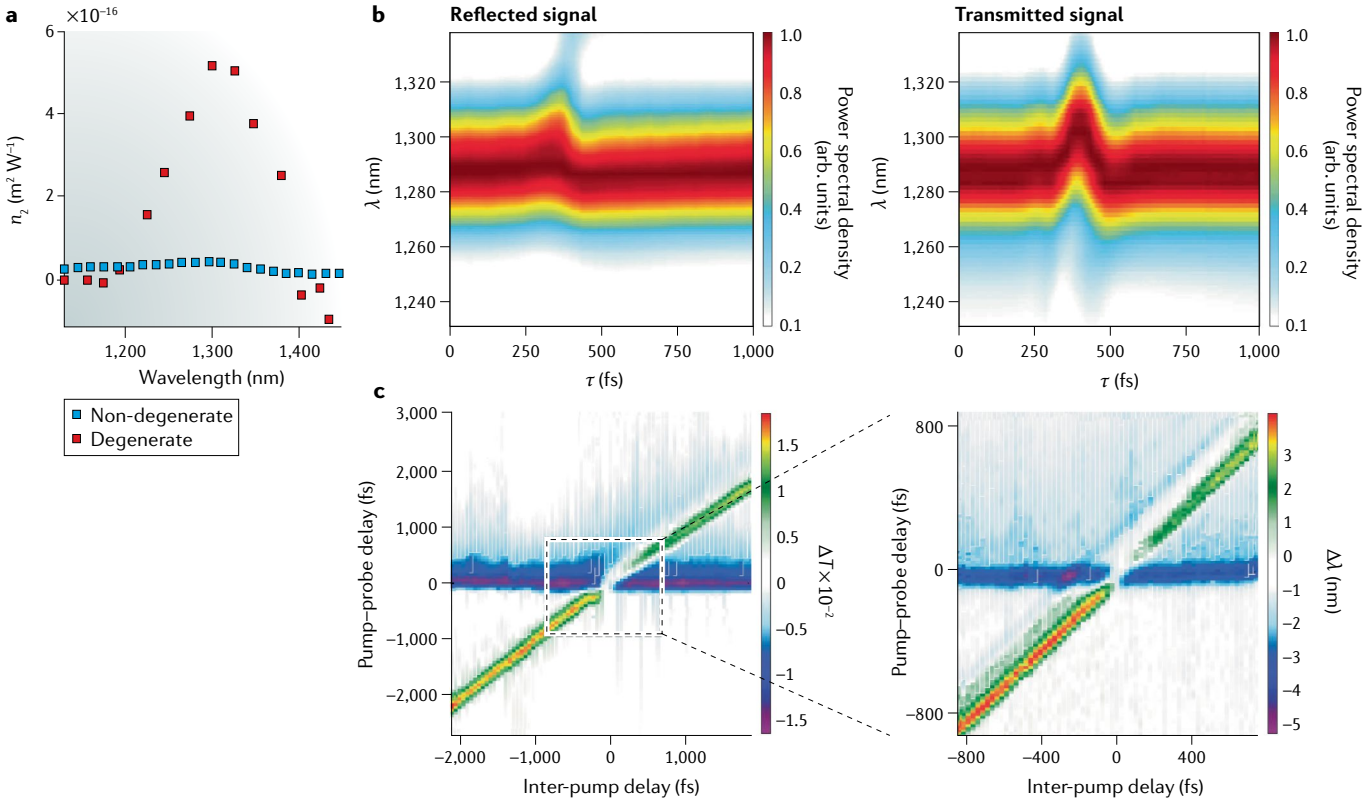


Fig. 6 | **Non-degenerate nonlinearities in aluminium-doped zinc oxide. a** | Wavelength dependence of the nonlinear refractive index $n_2$ of aluminium-doped zinc oxide (AZO) under degenerate (red) and non-degenerate (blue) excitation. The nonlinearity is optimally enhanced near the zero-permittivity wavelength $\lambda_{ZE}$ in the degenerate case. **b** | Transient spectrogram of the reflected and transmitted probe signals at a 1,290 nm central wavelength under near-IR (NIR) pump excitation as a function of pump–probe delay $\tau$. **c** | Change in the probe pulse transmission $T$ as a function of the pump–probe delay $\Delta\tau$ and the inter-pump delay $\Delta t$. The UV pump decreases the transmission, whereas the NIR pump increases it. The combined effect produces a $\Delta t$-dependent modulation. The measured shift of the central wavelength $\lambda$ of the transmitted probe pulse (approximately 15 nm bandwidth) in a region corresponding to the dashed box is also shown. The UV pump blueshifts the probe wavelength, whereas the NIR pump redshifts it. For $\Delta t = 0$, the two effects may even cancel out. Panel **a** is adapted from REF.[52], CC-BY-4.0. Panel **b** is adapted from REF.[137], CC-BY-3.0. Panel **c** is adapted from REF.[36], CC-BY-4.0.

at the zero-permittivity wavelength when compared with the value at other wavelengths.

We conclude this section by discussing an important series of experiments that provide some key physical insights into nonlinearities of Drude materials despite being performed away from the ENZ region[51,57,130]. A regular array of high-aspect-ratio ITO nanorods (180 nm wide × 2600 nm long) was fabricated on an yttria-stabilized zirconia substrate. In the IR, the samples featured localized surface plasmon resonances associated with the transverse dimension of the nanorods[57]. In the visible spectrum, the samples displayed a set of resonances corresponding to standing waves within propagating eigenmodes travelling along the length of the rods[51]. This single platform, therefore, offered an elegant opportunity to probe the nonlinear behaviour of a Drude material in both its dielectric ($\omega > \omega_p$) and metallic ($\omega < \omega_p$) spectral regions. In a first experiment, the device was optically excited at the surface plasmon resonance of the ITO nanoparticles ($\lambda = 1{,}500$ nm) to generate intraband excitations of conduction electrons, and probed in the MIR (3000–7000 nm)[57]. Large changes in absorption were reported, with extinction ratios of 6 dB at 3,900 nm on sub-picosecond timescales. The authors reported that the plasma frequency of ITO was being tuned from roughly 2 eV to 1.6 eV, and concluded that the response time was faster than that of metals owing to the high electron temperature, a direct consequence of the low electron density of ITO. In a follow-up study[51], the sample was pumped at 1,500 nm and probed in the visible range (360–710 nm), obtaining changes in transmission of up to 25% (1 dB) throughout the visible spectrum with a response time of 1.5 ps. They also performed the experiment with a pump centred at 800 nm, but observed a weaker response. They also observed a transient response with a 4 µs response time, which they attributed to a lattice-cooling response that is hindered by the length of the nanorods.

From these studies, we can conclude that in non-degenerate nonlinear interactions involving transparent conducting oxides, nonlinearities are enhanced when either the pump or the probe is set to the zero-permittivity wavelength. Pumping at the zero-permittivity wavelength can strongly modify the permittivity spectrum in the

ENZ region[37,138]. Experimental data seem to suggest that degenerate nonlinearities exhibit a modest enhancement in $\chi^{(3)}(\omega; \omega, \omega, -\omega)$ at the zero-permittivity wavelength[37]; non-degenerate nonlinearities do not seem to display a $\chi^{(3)}$ enhancement[13,60]. These enhancements, in addition to field enhancements, contribute to large changes in the refractive index: in the wavelength-degenerate case, this is equivalent to a large $n_2$. This change in refractive index also influences the reflective properties of the surface by modifying its optical wave impedance.

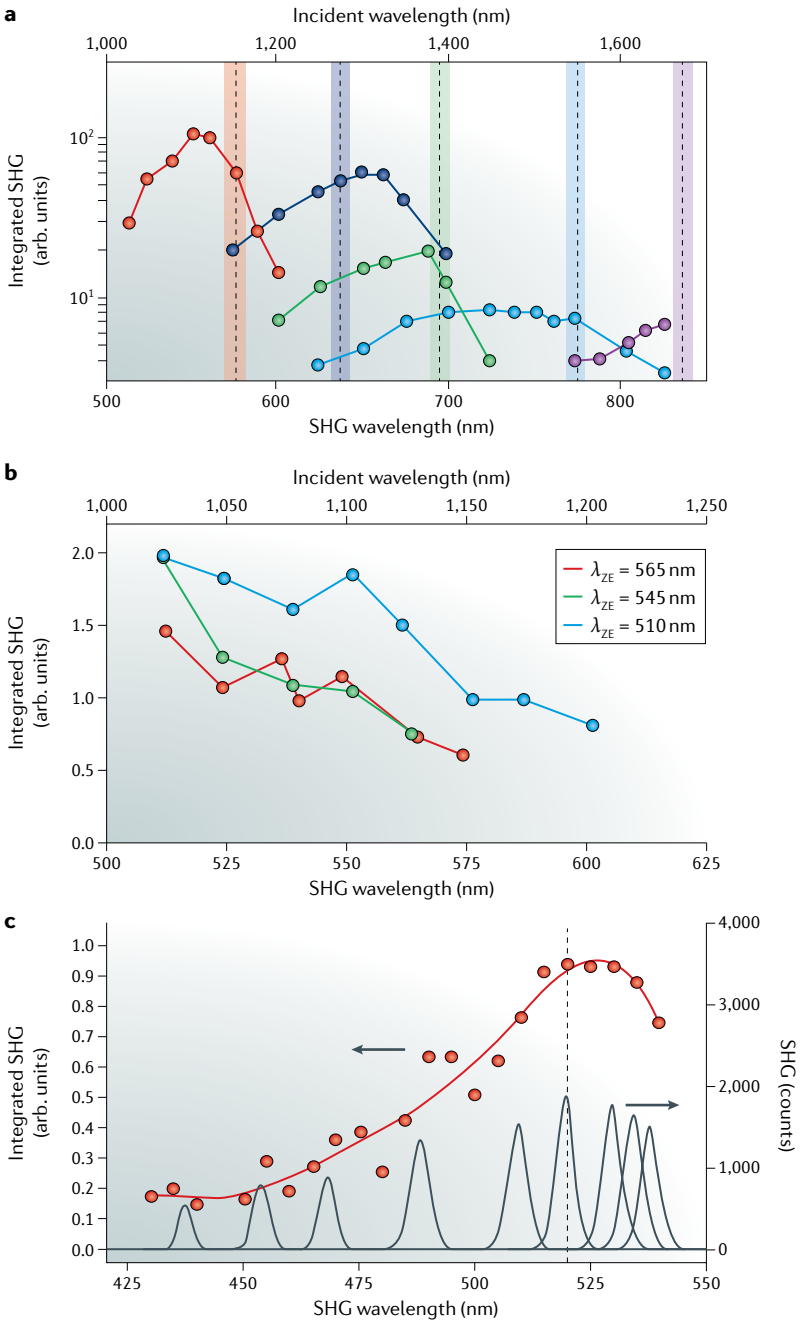


Fig. 7 | **Harmonic generation in epsilon-near-zero materials. a** | Second-harmonic generation (SHG) intensity as a function of the incident wavelength for indium tin oxide (ITO) films with zero-permittivity wavelengths, $\lambda_{ZE}$ (indicated by the vertical lines), equal to 1,150 nm (red), 1,270 nm (dark blue), 1,390 nm (green), 1,550 nm (blue) and 1,670 nm (violet). **b** | SHG intensities as a function of the incident wavelength for TiN thin films with $\lambda_{ZE}$ = 510 (blue), 545 (green) and 565 nm (red). **c** | SHG spectra for different excitation wavelengths in a TiN thin film (black curves). The zero-permittivity wavelength (vertical line) is at 520 nm. The dots are the integrated signal over these individual spectra, and the line is a polynomial fit. Panels **a** and **b** are adapted with permission from REF.[35], ACS. Panel **c** is adapted with permission from REF.[97], ACS.

### *Harmonic generation*

Prior to experiments, multiple theoretical works had predicted an enhancement of harmonic generation in ENZ and NZI media[27,28,30,141]; there is also some more recent microscopic modelling work on the topic[65,142,143]. It has been shown theoretically that in a strongly resonant system loaded with ITO operating under ENZ conditions, both the second-order nonlinear response due to free electrons and the third-order nonlinear response from bound electrons contribute to third-harmonic generation (THG)[144].

Two different groups independently reported an enhancement of THG in ITO at its zero-permittivity wavelength[10,11] demonstrating an ENZ-based nonlinear enhancement. The first paper showed that, when pumped at its zero-permittivity wavelength, a 37-nm-thick ITO film offers a third-harmonic conversion efficiency that is 600 times as large as that of a 300-μm-thick crystalline silicon wafer. Because these films are subwavelength in dimension along the propagation direction, phase-matching is not a great concern, even when matching frequencies multiple octaves apart. The measurements were performed using 150 fs pulses with a peak intensity of 40 MW cm$^{-2}$, and the sample was excited at 45° oblique incidence to provide a field enhancement. The THG third-order susceptibility was estimated to be $\chi^{(3)}_{zzzz} = 3.5 \times 10^{-18}$ m$^2$ V$^{-2}$, slightly larger than that of silicon[7]. In the second paper, the authors excited the ENZ mode of a 33-nm-thick ITO film in a Kretchsmann configuration using 50 fs pulses with a peak intensity of 20 GW cm$^{-2}$ (REF.[10]). The third-harmonic signal they observed was 200 times larger than that of the same film in a regular transmission geometry at oblique incidence; this difference was attributed to a sixfold field intensity enhancement for light propagating in the ENZ mode (for third-order effects, the output intensity scales with the cube of the enhancement of the fundamental intensity, and $6^3 \approx 200$). The signal from the Kretchsmann configuration was also four orders of magnitude larger than that generated by the glass that formed the coupling prism. The conversion efficiency was estimated to be $3.3 \times 10^{-6}$, and the third-order susceptibility, extracted using numerical models, was estimated at $\chi^{(3)}_{zzzz} = 3 \times 10^{-21}$ m$^2$ V$^{-2}$, a value valid only in the ENZ region. The large third-order nonlinear susceptibility of ITO was attributed to its large electron mobility.

In a related series of experiments, ENZ-based nonlinear enhancement has been used to increase second-order nonlinear effects[35,97]. Second-harmonic generation (SHG) was examined in two distinct ENZ platforms: an array of 37-nm-thick ITO films with zero-permittivity wavelengths ranging from 1,150 nm to 1,670 nm (FIG. 7a), and 40-nm-thick TiN films with zero-permittivity wavelengths ranging from 510 nm to 645 nm (FIG. 7b,c). It is worth noting that neither of these materials is expected to exhibit second-order effects because of their centrosymmetry[145,146]. Nevertheless,

a second-harmonic response was observed in both materials due to surface effects and nonlocal bulk effects. Pumping ITO at the zero-permittivity wavelength resulted in the generation of second-harmonic signals with conversion efficiencies comparable to those of a 500-μm-thick quartz crystal reference sample. The signal was large enough to enable the estimation of several elements of the second-order susceptibility tensor: $\chi^{(2)}_{zzz} = 1.8 \times 10^{-13}\,\mathrm{m\,V^{-1}}$ and $\chi^{(2)}_{zxx} = 0.5 \times 10^{-13}\,\mathrm{m\,V^{-1}}$. The generated nonlinear signal peaks at the zero-permittivity wavelength with a substantial reduction elsewhere, and the wavelength at which this signal enhancement appears scales with $\lambda_{ZE}$ (FIG. 7a).

Experiments on TiN involve a notable variation with respect to experiments on other materials: the zero-permittivity wavelength is at the harmonic rather than at the fundamental frequency. It is intriguing to consider whether the conversion efficiency can be increased not by enhancing one of the incident fields, but by enhancing the field of a generated nonlinear mode, as is often done in optical resonators[147,148]. A second-harmonic signal a factor of 50 smaller than that of ITO was reported. This difference was attributed to higher material losses in TiN (at the zero-permittivity wavelength, $\epsilon'' > 3$, compared with $\epsilon'' < 0.6$ for ITO), which produce a much smaller ENZ-based field enhancement. From the results of this study (FIG. 7b), it is not clear that there is a substantial ENZ-based nonlinear enhancement when the harmonic output field is set to the ENZ region. Further weakening the conclusions of this study is the fact that several TiN samples that were annealed below a certain temperature (corresponding to the samples with the longest zero-permittivity wavelengths) did not generate any observable second-harmonic signal[35]. In a more recent study, harmonic generation was studied with the ENZ region set to the harmonic frequency. SHG was characterized in a thin TiN film with a zero-permittivity wavelength of 520 nm pumped at normal incidence[97], and an enhancement of SHG by a factor of 5 relative to measurements at shorter wavelengths was reported (fundamental frequency at 880 nm, SHG at 440 nm; FIG. 7c). Structuring the TiN films into U-shaped antennas supporting localized surface plasmon resonances centred at the fundamental frequency provided an additional field enhancement for the nonlinear interaction, generating a nonlinear signal up to 16 times that of the bare unstructured film, in addition to the fivefold enhancement already mentioned. Combining the two effects, the total conversion efficiency was estimated to be of the order of $10^{-12}$.

Finally, a periodically structured metal–dielectric–metal structure incorporating both ITO and TiN (REF.[129]) was used to demonstrate a 50,000-fold enhancement of SHG[149].

### *Static-field control of permittivity*

Perhaps most interesting from the applications perspective is that the complex refractive index of ITO can be modulated by an applied voltage. A thin layer of ITO bounded by a dielectric can exhibit a change in refractive index of order unity as a response to a static electric field[38] (FIG. 8a). This effect results from a dense charge accumulation (or depletion) region that builds up tightly confined to the ITO–dielectric boundary in the presence of an applied voltage. From a Drude–Lorentz model, it can be shown that the change in refractive index takes the form:

$$\Delta n = \frac{-e^2\lambda_0^2}{8\pi^2 c^2 \epsilon_0 n}\left(\frac{\Delta n_e}{m_e^*} + \frac{\Delta p}{m_h^*}\right) \quad (8)$$

where $\Delta n_e$ and $\Delta p$ are the excess electron and hole densities in the charge accumulation region, and $m_h^*$ the hole effective mass. This expression suggests that the change in refractive index is enhanced in ENZ and NZI materials. This principle was exploited to demonstrate wide-range optical phase modulation at telecommunication wavelengths in electrically tunable conducting metasurfaces based on an ITO substrate operating within the ENZ region[39,40]. The architecture of the devices consisted of a metal–oxide–semiconductor heterostructure, with the metallic metasurface and ITO layer acting as the metal and semiconductor layers, respectively. The device was designed to enable a large optical field confinement in the ITO layer, making the response very sensitive to changes in the permittivity of ITO. Using this technique, a dynamic beam-steering device was developed based on an electrically tunable Au/dielectric gate/ITO grating metasurface with $Al_2O_3$ as the dielectric gate[39]. Continuous optical phase modulation ranging from 0° to 303° was demonstrated in a reflective aluminium fishbone metasurface[40] featuring a dual-gated Al/dielectric gate/ITO/dielectric gate heterostructure on an Al back reflector (FIG. 8b), and using an $Al_2O_3$/$HfO_2$ nano-laminate dielectric gate grown by atomic layer deposition.

A device based on all-dielectric Huygens metasurfaces that exploits this principle[132] was used to demonstrate a modulation of the absolute transmission from 0.71 to 0.42 as the bias voltage was changed from 10 V to −10 V (FIG. 8c).

Finally, an ENZ-based silicon–photonic electroabsorption modulator that also exploits a voltage-tunable permittivity was demonstrated[41]. The device was operated at wavelengths much shorter than the zero-permittivity wavelength of the ITO film ($\lambda_{ZE}$ = 6,300 nm). During operation, the applied voltage increased the carrier concentration and raised the plasma frequency, so that the zero-permittivity wavelength coincided with the operating wavelength. The device was 4 μm long, featured a broadband (1,530–1,590 nm) extinction of 6.5 dB and could modulate at rates of 2.5 Gb $s^{-1}$.

### *Other nonlinear phenomena*

Aside from nonlinear enhancements to refraction and harmonic generation, ENZ and NZI materials have enabled the realization of many other nonlinear optical effects. Some are discussed below.

The Berreman mode of a 75-nm-thick film of indium-doped cadmium oxide with a zero-permittivity wavelength of $\lambda_{ZE}$ = 2,100 nm was used to demonstrate polarization switching with an extinction ratio of almost 20 dB (REF.[14]) (FIG. 9a). The Berreman mode acted as a plasmonic cavity for the device, providing 14 times as much absorption as a single pass through the film. The plasma

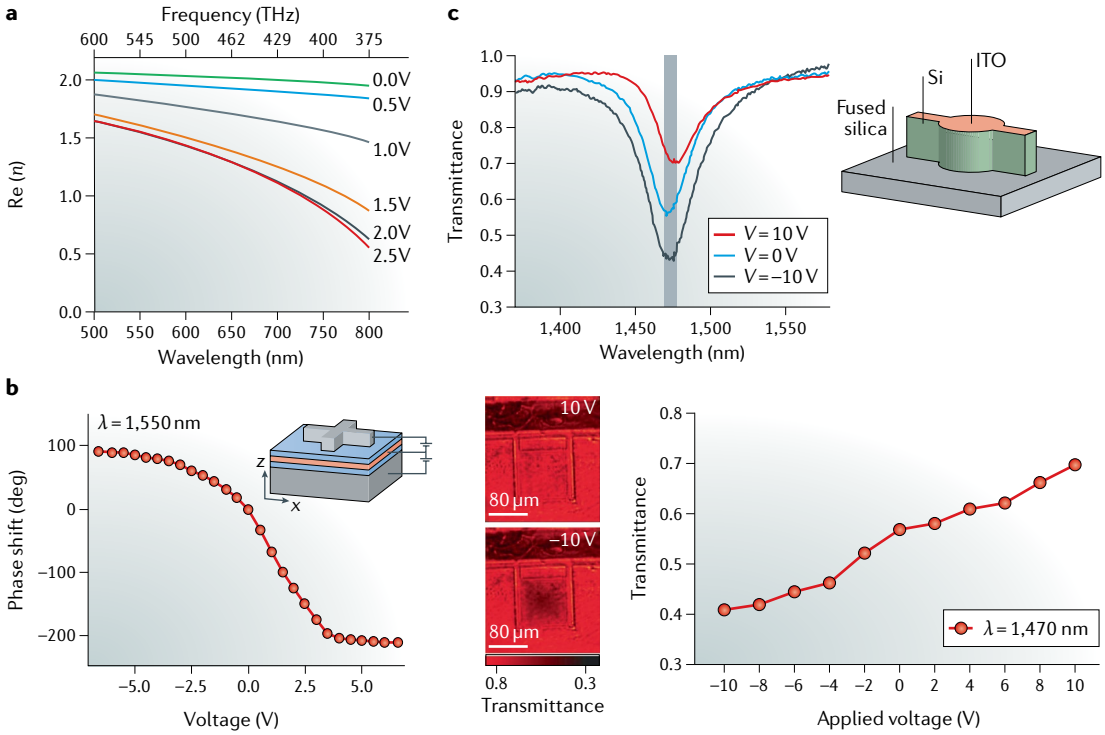


Fig. 8 | **Voltage-controlled permittivity. a** | The real part of the refractive index *n* of a 5-nm accumulation layer on the surface of indium tin oxide (ITO) under different applied voltages. **b** | Measured phase shift of a reflective aluminium fishbone metasurface as a function of applied voltage at a wavelength of $\lambda = 1{,}550$ nm. A single unit cell of the metasurface is shown in the inset. **c** | Experimental transmittance (*T*) spectrum of a silicon Huygens metasurface capped with an ITO film at three distinct applied gate bias voltages *V*. A single unit cell of the metasurface is shown in the inset. As seen in the lower part, the peak transmittance amplitude is tuned with *V*. The grey vertical bar indicates the wavelength at which the IR camera images were taken. These images, which use monochromatic light, show the device at two bias voltages at the working wavelength of the device. Panel **a** is adapted with permission from REF.[38], ACS. Panel **b** is adapted with permission from REF.[40], ACS. Panel **c** is adapted with permission from REF.[132], Optical Society of America.

frequency was modulated from $\omega_p = 2.11 \times 10^{15}$ rad s$^{-1}$ to $1.96 \times 10^{15}$ rad s$^{-1}$ (that is, from 1.39 eV to 1.29 eV) following the activation of the probe beam before the system made a full recovery to its initial state within 800 fs.

Polarization switching was also demonstrated in a planar plasmonic cavity consisting of an array of gold nanoparticles separated from a planar gold film by a 10-nm-thick ITO layer[131]. This structure has a distinctly polarization-dependent response, with the planar cavity modes appearing only for p-polarized illumination. Pumping on resonance ($\lambda = 645$ nm) results in a maximum relative change in reflectance $\Delta R/R \approx 75\%$. This effect enabled polarization switching with induced phase differences exceeding 20° on an ultrafast timescale. This platform also enabled all-optical modulation on the order of 1–2 dB (REF.[150]).

In related work, the resonance wavelength of a Fabry–Pérot cavity was tuned by 200 nm using a 70-nm-thick active ENZ layer[151]. The shift was attributed to a modulation of the plasma frequency from 1.85 eV to 1.70 eV.

Finally, NZI materials provide unique opportunities for realizing phase-matching for nonlinearities. A light field propagating in a material with a vanishing refractive index has a directionless **k**-vector (that is, $\mathbf{k} = \vec{0}$). As a consequence, in a nonlinear interaction beams can be mixed in any direction while satisfying phase-matching conditions, sometimes even simultaneously. This can be derived explicitly by calculating the phase mismatch for the same four-wave mixing process for a forward-propagating and a backward-propagating signal:

$$\Delta\mathbf{k}_{FW} = \mathbf{k}_p + \mathbf{k}_p - \mathbf{k}_s - \mathbf{k}_i$$
$$\Delta\mathbf{k}_{BW} = \mathbf{k}_p + \mathbf{k}_p + \mathbf{k}_s - \mathbf{k}_i \quad (9)$$

where $\mathbf{k}_p$, $\mathbf{k}_s$ and $\mathbf{k}_i$ are the momentum vectors for the pump, signal and idler photons, respectively. If $\Delta\mathbf{k}_{FW} = 0$, then necessarily $\Delta\mathbf{k}_{BW} \approx 2|\mathbf{k}_s|$, which can only equal zero if the refractive index equals zero at the signal wavelength. This effect was demonstrated using a pair of 800-nm-thick zero-index metamaterial fishnet structures with $\lambda_{ZI} = 1340$ nm and 1460 nm (REF.[152]). The metamaterial was excited using 100 fs pulses, which resulted in a spectrally broadened output in both the forward-propagating and backward-propagating directions. At wavelengths nearest to the zero-index wavelength, the nonlinear generated signals were of comparable magnitude (FIG. 9b,c). A similar effect was predicted in Dirac-cone zero-index metamaterials for SHG[153] and four-wave mixing[154] processes, and was demonstrated in a degenerate four-wave-mixing nonlinearity in a 500-nm-thick AZO sample[62]. Note that nonlinear interactions in NZI media continue to necessitate that phase-matching

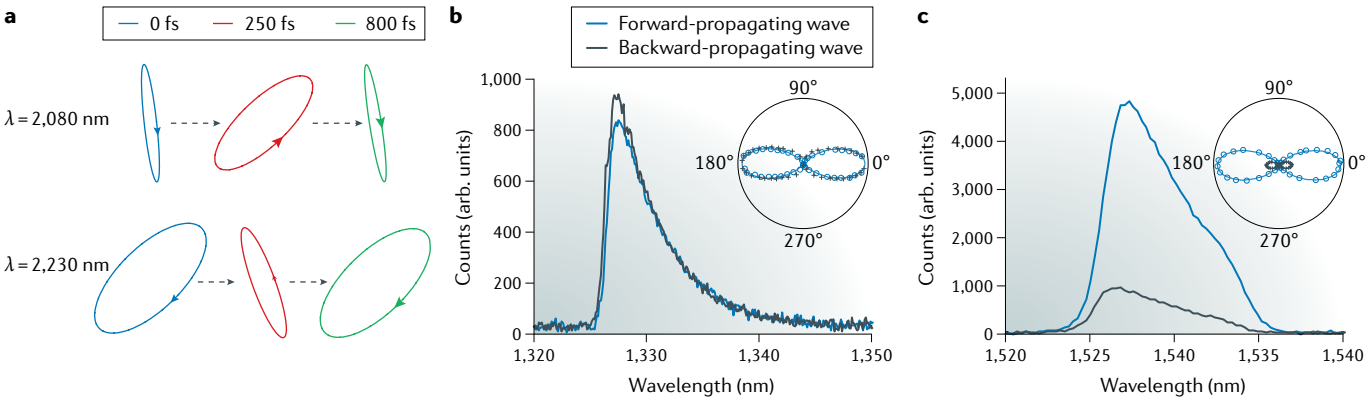


Fig. 9 | **Other nonlinear phenomena in epsilon-near-zero and near-zero-index materials. a** | The measured polarization ellipse of a beam reflected from the Berreman mode of a doped CdO film (zero-permittivity wavelength $\lambda_{ZE} = 2{,}100$ nm) at $\lambda = 2{,}080$ nm and 2,230 nm at delay times of 0, 250 fs and 800 fs. The reflected wave is initially elliptically polarized clockwise (blue); after the pump pulse the reflected wave is still elliptical, but rotated anticlockwise (red), and it finally recovers its original state (green). **b** | In the zero-index regime of a near-zero-index fishnet metamaterial, the four-wave mixing (FWM) process generates the same nonlinear yield for forward-propagating waves (blue) as backward-propagating waves (black), illustrating directionless phase-matching. **c** | By contrast, in the negative-index regime, FWM for forward-propagating waves is much stronger than for backward-propagating waves as a result of phase mismatch. Insets in panels **b** and **c** show the dependence of the nonlinear emission (with a horizontally polarized analyser) on pump polarization, which has the characteristic $\cos^6\theta$ curve of $\chi^{(3)}$ dynamics. Panel **a** is adapted from REF.[14], Springer Nature Limited. Panels **b** and **c** are adapted with permission from REF.[152], AAAS.

conditions are satisfied; however, beams may enter and leave the interaction region in multiple simultaneous directions while still satisfying these conditions.

## Conclusions and perspectives

We have reviewed the work that has been done thus far in exploiting ENZ and NZI responses for various nonlinear optical effects. The experimental results support the conclusion that ENZ materials provide a significant enhancement to ultrafast nonlinearities, particularly in regard to the intensity-dependent index of refraction[12,52,61] and harmonic generation[10,11,35]. The enhancement can be accessed when the material is pumped or probed at the zero-permittivity wavelength. ENZ effects can also enhance nonlinearities at frequencies different to those of the incident fields, such as when the zero-permittivity wavelength coincides with a harmonic of the pump field[97]. Reported spectra of $\chi^{(3)}(\omega; \omega, \omega, -\omega)$ (the term associated with $n_2$) often show a small peak at the zero-permittivity wavelength[52]; however, the field-enhancement mechanism due to the continuity of the electric field plays a more important role in enhancing nonlinearities, particularly at oblique angles. In one specific case featuring an ENZ metamaterial, an angle-dependent field enhancement was also observed[135]. Altogether, these results demonstrate the promise and limitations of ENZ-based enhancements. Despite the fact that ENZ materials have made accessible a new regime of ultrafast nonlinear effects, much work remains to be done before conceptual laboratory demonstrations can lead to practical devices.

With respect to bulk ENZ materials, the main obstacle is an issue of material engineering: there is no single material that is as ubiquitous in ENZ-nonlinear optical interactions as silicon is in electronics. Most studies have focused on ITO and AZO; yet both materials have clear limitations, such as optical losses and fabrication processes with low reproducibility. There might, of course, be a better material platform that is still to be discovered. The ideal material would have the following properties: CMOS compatibility, high degree of crystallinity, large carrier mobility and low linear losses. If possible, this material would have also a tailorable zero-permittivity wavelength, and it would be straightforward to deposit and nanostructure. Many materials check a few of these boxes, but none so far meets all of these criteria. Thus, considerable effort is still required to enable an ENZ material platform that can pave the way for the development of practical and cost-effective nonlinear optical devices.

The problem of material losses deserves special attention[155]. The ENZ materials that have been discussed all exhibit considerable losses, which for the best case results in an optical attenuation of roughly 4 dB μm$^{-1}$ (corresponding to $\mathrm{Im}(n) = 0.1$) in the NIR. For certain nonlinear applications, some loss may be tolerable. However, high losses will ultimately limit the scope of practical applications. Polar dielectrics whose ENZ regions originate from phononic resonances tend to have smaller imaginary parts at their respective zero-permittivity wavelengths, although the ratio of the zero-permittivity wavelength to the imaginary part of $n$ is similar to the value in the NIR[95,103]. Metamaterials with an ENZ or NZI region could also be engineered from all-dielectric components to exhibit minimal resistive losses, and for virtually any target wavelength[122]. However, neither of these platforms has yet conclusively demonstrated ENZ-based nonlinear enhancements, despite some predictions[25,156]. Gain media have successfully been integrated in some plasmonics applications, alleviating to some extent the large losses of those systems, and could perhaps also be of use here[157,158]. Some theoretical

works proposed the incorporation of gain media in metal–dielectric composite-based ENZ metamaterials with a specific focus on nonlinear processes, finding that in these systems loss could be compensated while still enabling low-threshold nonlinear effects[159,160]. So far, experimental demonstrations are lacking.

As mentioned, a few open questions remain in this budding field, in particular regarding the roles of the mechanisms outlined for the different nonlinearities. These questions include whether phonon-based ENZ regions also greatly enhance nonlinearities; whether hot electron effects are expected to be pulse-width-dependent; how the pulse duration affects the nonlinearities and bandwidths of ENZ materials; and whether other nonlinear effects and equations will need to be reconsidered in the presence of a vanishing permittivity, as happened for the intensity-dependent index of refraction[48]. Finally, multiple exciting predictions of nonlinear effects remain to be confirmed in both ENZ and NZI materials, including cavity-free stopped light and self-trapping beams with unique soliton solutions[79,161]. ENZ materials have also been predicted to enhance spontaneous emission and superradiance[162,163], with the spontaneous emission even predicted to be controllable through modulation of the Purcell effect[164]. Finally, there have been several proposals to use ITO or another ENZ material for all-optical[165–167] and electro-optical[168–170] modulators and switches. Experimental demonstrations of these devices could help to advance our understanding and ability to further develop this intriguing class of materials.

Despite the challenges mentioned above, the prospects of applications for ENZ nonlinear media are exciting and have great potential in the fields of nanophotonics and nonlinear optics. Several convincing laboratory demonstrations and proofs of concept have been reported regarding the extremely large nonlinear optical response of ENZ materials and their potential for applications. Based on the research activity in this field, and considering the constant advances in material fabrication and nanofabrication, we anticipate that research on the nonlinear optical response of ENZ materials will generate important results for years to come.

Published online 21 June 2019


1. Garmire, E. Nonlinear optics in daily life. *Opt. Express* **21**, 30532–30544 (2013).
2. Cotter, D. et al. Nonlinear optics for high-speed digital information processing. *Science* **286**, 1523–1528 (1999).
3. Glezer, E. N. et al. Three-dimensional optical storage inside transparent materials. *Opt. Lett.* **21**, 2023–2025 (1996).
4. Mukamel, S. *Principles of Nonlinear Optical Spectroscopy* (Oxford Univ. Press, 1999).
5. Leach, J. et al. Quantum correlations in optical angle-orbital angular momentum variables. *Science* **329**, 662–665 (2010).
6. Howell, J. C., Bennink, R. S., Bentley, S. J. & Boyd, R. W. Realization of the Einstein–Podolsky–Rosen paradox using momentum-and position-entangled photons from spontaneous parametric down conversion. *Phys. Rev. Lett.* **92**, 210403 (2004).
7. Boyd, R. W. *Nonlinear Optics*. 3rd edn (Academic, 2008).
8. Miller, D. A. B. Are optical transistors the logical next step? *Nat. Photonics* **4**, 3–5 (2010).
9. Kinsey, N. et al. Epsilon-near-zero Al-doped ZnO for ultrafast switching at telecom wavelengths. *Optica* **2**, 616–622 (2015).
10. Luk, T. S. et al. Enhanced third harmonic generation from the epsilon-near-zero modes of ultrathin films. *Appl. Phys. Lett.* **106**, 151103 (2015).
11. Capretti, A., Wang, Y., Engheta, N. & Dal Negro, L. Enhanced third-harmonic generation in Si-compatible epsilon-near-zero indium tin oxide nanolayers. *Opt. Lett.* **40**, 1500–1503 (2015).
12. Alam, M. Z., De Leon, I. & Boyd, R. W. Large optical nonlinearity of indium tin oxide in its epsilon-near-zero region. *Science* **352**, 795–797 (2016).
13. Caspani, L. et al. Enhanced nonlinear refractive index in $\epsilon$-near-zero materials. *Phys. Rev. Lett.* **116**, 233901 (2016).
14. Yang, Y. et al. Femtosecond optical polarization switching using a cadmium oxide-based perfect absorber. *Nat. Photonics* **11**, 390–395 (2017).
15. Silveirinha, M. & Engheta, N. Tunneling of electromagnetic energy through subwavelength channels and bends using $\epsilon$-near-zero materials. *Phys. Rev. Lett.* **97**, 157403 (2006).
16. Alù, A., Silveirinha, M. G., Salandrino, A. & Engheta, N. Epsilon-near-zero metamaterials and electromagnetic sources: tailoring the radiation phase pattern. *Phys. Rev. B* **75**, 155410 (2007).
17. Edwards, B., Alù, A., Young, M. E., Silveirinha, M. & Engheta, N. Experimental verification of epsilon-near-zero metamaterial coupling and energy squeezing using a microwave waveguide. *Phys. Rev. Lett.* **100**, 033903 (2008).
18. Molesky, S., Dewalt, C. J. & Jacob, Z. High temperature epsilon-near-zero and epsilon-near-pole metamaterial emitters for thermophotovoltaics. *Opt. Express* **21**, A96–A110 (2013).
19. Engheta, N. Pursuing near-zero response. *Science* **340**, 286–287 (2013).
20. Niu, X., Hu, X., Chu, S. & Gong, Q. Epsilon-near-zero photonics: a new platform for integrated devices. *Adv. Opt. Mater.* **6**, 1701292 (2018).
21. Liberal, I. & Engheta, N. The rise of near-zero-index technologies. *Science* **358**, 1540–1541 (2017).
22. Liberal, I. & Engheta, N. Zero-index platforms: where light defies geometry. *Opt. Photon. News* **27**, 26–33 (2016).
23. Liberal, I. & Engheta, N. Near-zero refractive index photonics. *Nat. Photonics* **11**, 149–158 (2017).
24. Vulis, D. I., Reshef, O., Camayd-Muñoz, P. & Mazur, E. Manipulating the flow of light using Dirac-cone zero-index metamaterials. *Rep. Prog. Phys.* **82**, 012001 (2019).
25. Ciattoni, A., Rizza, C. & Palange, E. Extreme nonlinear electrodynamics in metamaterials with very small linear dielectric permittivity. *Phys. Rev. A* **81**, 043839 (2010).
26. Ciattoni, A., Rizza, C. & Palange, E. Transmissivity directional hysteresis of a nonlinear metamaterial slab with very small linear permittivity. *Opt. Lett.* **35**, 2130–2132 (2010).
27. Vincenti, M. A., de Ceglia, D., Ciattoni, A. & Scalora, M. Singularity-driven second-and third-harmonic generation at $\epsilon$-near-zero crossing points. *Phys. Rev. A* **84**, 63826 (2011).
28. Ciattoni, A. & Spinozzi, E. Efficient second-harmonic generation in micrometer-thick slabs with indefinite permittivity. *Phys. Rev. A* **85**, 043806 (2012).
29. Argyropoulos, C., Chen, P.-Y., D'Aguanno, G., Engheta, N. & Alù, A. Boosting optical nonlinearities in $\epsilon$-near-zero plasmonic channels. *Phys. Rev. B* **85**, 045129 (2012).
30. Argyropoulos, C., D'Aguanno, G. & Alù, A. Giant second-harmonic generation efficiency and ideal phase matching with a double $\epsilon$-near-zero cross-slit metamaterial. *Phys. Rev. B* **89**, 235401 (2014).
31. Harbold, J. M. et al. Highly nonlinear As–S–Se glasses for all-optical switching. *Opt. Lett.* **27**, 119–121 (2002).
32. Slusher, R. E. et al. Large Raman gain and nonlinear phase shifts in high-purity $As_2Se_3$ chalcogenide fibers. *J. Opt. Soc. Am. B* **21**, 1146–1155 (2004).
33. Eggleton, B. J., Luther-Davies, B. & Richardson, K. Chalcogenide photonics. *Nat. Photonics* **5**, 141–148 (2011).
34. Li, G., Zhang, S. & Zentgraf, T. Nonlinear photonic metasurfaces. *Nat. Rev. Mater.* **2**, 17010 (2017).
35. Capretti, A., Wang, Y., Engheta, N. & Dal Negro, L. Comparative study of second-harmonic generation from epsilon-near-zero indium tin oxide and titanium nitride nanolayers excited in the near-infrared spectral range. *ACS Photonics* **2**, 1584–1591 (2015).
36. Clerici, M. et al. Controlling hybrid nonlinearities in transparent conducting oxides via two-colour excitation. *Nat. Commun.* **8**, 15829 (2017).
37. Carnemolla, E. G. et al. Giant nonlinear frequency shift in epsilon-near-zero aluminum zinc oxide thin films. *Conference on Lasers and Electro-Optics*, SM4D.7. (OSA, 2018).
38. Feigenbaum, E., Diest, K. & Atwater, H. A. Unity-order index change in transparent conducting oxides at visible frequencies. *Nano Lett.* **10**, 2111–2116 (2010).
39. Huang, Y.-w et al. Gate-tunable conducting oxide metasurfaces. *Nano Lett.* **16**, 5319–5325 (2016).
40. Kafaie Shirmanesh, G., Sokhoyan, R., Pala, R. A. & Atwater, H. A. Dual-gated active metasurface at 1550 nm with wide (300°) phase tunability. *Nano Lett.* **18**, 2957–2963 (2018).
41. Wood, M. G. et al. Gigahertz speed operation of epsilon-near-zero silicon photonic modulators. *Optica* **5**, 233–236 (2018).
42. Li, E., Gao, Q., Chen, R. T. & Wang, A. X. Ultracompact silicon-conductive oxide nanocavity modulator with 0.02 lambda-cubic active volume. *Nano Lett.* **18**, 1075–1081 (2018).
43. Liu, X. et al. Epsilon-near-zero Si slot-waveguide modulator. *ACS Photonics* **5**, 4484–4490 (2018).
44. Li, Y. et al. On-chip zero-index metamaterials. *Nat. Photonics* **9**, 738–742 (2015).
45. Noginov, M. A. et al. Transparent conductive oxides: plasmonic materials for telecom wavelengths. *Appl. Phys. Lett.* **99**, 2009–2012 (2011).
46. Stegeman, G. I., Wright, E. M., Finlayson, N., Zanoni, R. & Seaton, C. T. Third order nonlinear integrated optics. *J. Light. Technol.* **6**, 953–970 (1988).
47. Eggleton, B. J. et al. Photonic chip based ultrafast optical processing based on high nonlinearity dispersion engineered chalcogenide waveguides. *Laser Photonics Rev.* **6**, 97–114 (2012).
48. Reshef, O. et al. Beyond the perturbative description of the nonlinear optical response of low-index materials. *Opt. Lett.* **42**, 3225–3228 (2017).
49. Maier, S. A. *Plasmonics: Fundamentals and Applications*. (Springer, 2007).
50. Derkachova, A., Kolwas, K. & Demchenko, I. Dielectric function for gold in plasmonics applications: size dependence of plasmon resonance frequencies and damping rates for nanospheres. *Plasmonics* **11**, 941–951 (2016).
51. Guo, P. et al. Large optical nonlinearity of ITO nanorods for sub-picosecond all-optical modulation of the full-visible spectrum. *Nat. Commun.* **7**, 12892 (2016).
52. Carnemolla, E. G. et al. Degenerate optical nonlinear enhancement in epsilon-near-zero transparent conducting oxides. *Opt. Mater. Express* **8**, 3392–3400 (2018).
53. Iyer, P. P., Pendharkar, M., Palmstrøm, C. J. & Schuller, J. A. Ultrawide thermal free-carrier tuning

of dielectric antennas coupled to epsilon-near-zero substrates. *Nat. Commun.* **8**, 472 (2017).
54. Liu, X. et al. Tuning of plasmons in transparent conductive oxides by carrier accumulation. *ACS Photonics* **5**, 1493–1498 (2018).
55. Elim, H. I., Ji, W. & Zhu, F. Carrier concentration dependence of optical Kerr nonlinearity in indium tin oxide films. *Appl. Phys. B* **82**, 439–442 (2006).
56. Liu, X. et al. Quantification and impact of nonparabolicity of the conduction band of indium tin oxide on its plasmonic properties. *Appl. Phys. Lett.* **105**, 181117 (2014).
57. Guo, P., Schaller, R. D., Ketterson, J. B. & Chang, R. P. Ultrafast switching of tunable infrared plasmons in indium tin oxide nanorod arrays with large absolute amplitude. *Nat. Photonics* **10**, 267–273 (2016).
58. de Ceglia, D. et al. Viscoelastic optical nonlocality of low-loss epsilon-near-zero nanofilms. *Sci. Rep.* **8**, 9335 (2018).
59. Dinu, M., Quochi, F. & Garcia, H. Third-order nonlinearities in silicon at telecom wavelengths. *Appl. Phys. Lett.* **82**, 2954–2956 (2003).
60. Kaipurath, R. M. et al. Optically induced metal-to-dielectric transition in epsilon-near-zero metamaterials. *Sci. Rep.* **6**, 27700 (2016).
61. Lee, Y. U. et al. Strong nonlinear optical response in the visible spectral range with epsilon-near-zero organic thin films. *Adv. Opt. Mater.* **6**, 1701400 (2018).
62. Vezzoli, S. et al. Optical time reversal from time-dependent epsilon-near-zero media. *Phys. Rev. Lett.* **120**, 043902 (2017).
63. Campione, S., de Ceglia, D., Vincenti, M. A., Scalora, M. & Capolino, F. Electric field enhancement in $\epsilon$-near-zero slabs under TM-polarized oblique incidence. *Phys. Rev. B* **87**, 035120 (2013).
64. Kamandi, M., Guclu, C., Luk, T. S., Wang, G. T. & Capolino, F. Giant field enhancement in longitudinal epsilon-near-zero films. *Phys. Rev. B* **95**, 161105(R) (2017).
65. Vincenti, M. A. et al. Second-harmonic generation in longitudinal epsilon-near-zero materials. *Phys. Rev. B* **96**, 045438 (2017).
66. Taliercio, T., Guilengui, V. N., Cerutti, L., Tournié, E. & Greffet, J.-J. Brewster 'mode' in highly doped semiconductor layers: an all-optical technique to monitor doping concentration. *Opt. Express* **22**, 24294–24303 (2014).
67. Vassant, S., Hugonin, J.-P., Marquier, F. & Greffet, J.-J. Berreman mode and epsilon near zero mode. *Opt. Express* **20**, 23971–23977 (2012).
68. Luk, T. S. et al. Directional perfect absorption using deep subwavelength low-permittivity films. *Phys. Rev. B* **90**, 085411 (2014).
69. Newman, W. D. et al. Ferrell–Berreman modes in plasmonic epsilon-near-zero media. *ACS Photonics* **2**, 2–7 (2014).
70. Bello, F. et al. Combining $\epsilon$-near-zero behavior and stopped light energy bands for ultra-low reflection and reduced dispersion of slow light. *Sci. Rep.* **7**, 8702 (2017).
71. Campione, S., Brener, I. & Marquier, F. Theory of epsilon-near-zero modes in ultrathin films. *Phys. Rev. B* **91**, 121408 (2015).
72. Berini, P. Long-range surface plasmon polaritons. *Adv. Opt. Photonics* **1**, 484–588 (2009).
73. Silveirinha, M. G. & Engheta, N. Theory of supercoupling, squeezing wave energy, and field confinement in narrow channels and tight bends using $\epsilon$-near-zero metamaterials. *Phys. Rev. B* **76**, 245109 (2007).
74. Javani, M. H. & Stockman, M. I. Real and imaginary properties of epsilon-near-zero materials. *Phys. Rev. Lett.* **117**, 107404 (2016).
75. Hamachi, Y., Kubo, S. & Baba, T. Slow light with low dispersion and nonlinear enhancement in a lattice-shifted photonic crystal waveguide. *Opt. Lett.* **34**, 1072–1074 (2009).
76. Monat, C. et al. Four-wave mixing in slow light engineered silicon photonic crystal waveguides. *Opt. Express* **18**, 22915–22927 (2010).
77. Boyd, R. W. Material slow light and structural slow light: similarities and differences for nonlinear optics [Invited]. *J. Opt. Soc. Am. B* **28**, A38–A44 (2011).
78. Powell, D. A. et al. Nonlinear control of tunneling through an epsilon-near-zero channel. *Phys. Rev. B* **79**, 245135 (2009).
79. Marini, A. & Garcia De Abajo, F. J. Self-organization of frozen light in near-zero-index media with cubic nonlinearity. *Sci. Rep.* **6**, 20088 (2016).
80. Khurgin, J. B. Everything is slow light. In *Optical, Opto-Atomic, and Entanglement-Enhanced Precision Metrology* vol. 10934, 109340 W (International Society for Optics and Photonics, 2019).
81. Johnson, P. B. & Christy, R. W. Optical constants of the noble metals. *Phys. Rev. B* **6**, 4370–4379 (1972).
82. Johnson, P. & Christy, R. Optical constants of transition metals: Ti, V, Cr, Mn, Fe, Co, Ni, and Pd. *Phys. Rev. B* **9**, 5056–5070 (1974).
83. Reutzel, M., Li, A., Gumhalter, B. & Petek, H. Excitation of two-photon photoemission where epsilon is near zero on Ag (111). Preprint at *arXiv* https://arxiv.org/abs/1809.02101 (2018).
84. West, P. R. et al. Searching for better plasmonic materials. *Laser Photonics Rev.* **4**, 795–808 (2010).
85. Naik, G. V., Shalaev, V. M. & Boltasseva, A. Alternative plasmonic materials: beyond gold and silver. *Adv. Mater.* **25**, 3264–3294 (2013).
86. Naik, G. V., Kim, J. & Boltasseva, A. Oxides and nitrides as alternative plasmonic materials in the optical range. *Opt. Mater. Express* **1**, 1090–1099 (2011).
87. Pradhan, A. K. et al. Extreme tunability in aluminum doped zinc oxide plasmonic materials for near-infrared applications. *Sci. Rep.* **4**, 6415 (2014).
88. Calzolari, A., Ruini, A. & Catellani, A. Transparent conductive oxides as near-IR plasmonic materials: the case of Al-doped ZnO derivatives. *ACS Photonics* **1**, 703–709 (2014).
89. Riley, C. T. et al. High-quality, ultraconformal aluminum-doped zinc oxide nanoplasmonic and hyperbolic metamaterials. *Small* **12**, 892–901 (2016).
90. Guo, Q. et al. A solution-processed ultrafast optical switch based on a nanostructured epsilon-near-zero medium. *Adv. Mater.* **29**, 1700754 (2017).
91. Wang, Y. et al. Tunability of indium tin oxide materials for mid-infrared plasmonics applications. *Opt. Mater. Express* **7**, 2727–2739 (2017).
92. Shkondin, E. et al. Large-scale high aspect ratio Al-doped ZnO nanopillars arrays as anisotropic metamaterials. *Opt. Mater. Express* **7**, 1606–1627 (2017).
93. Anopchenko, A., Tao, L., Arndt, C. & Lee, H. W. H. Field-effect tunable and broadband epsilon-near-zero perfect absorbers with deep subwavelength thickness. *ACS Photonics* **5**, 2631–2637 (2018).
94. Anopchenko, A., Gurung, S., Tao, L., Arndt, C. & Lee, H. W. H. Atomic layer deposition of ultra-thin and smooth Al-doped ZnO for zero-index photonics. *Mater. Res. Express* **5**, 014012 (2018).
95. Caldwell, J. D. et al. Low-loss, infrared and terahertz nanophotonics using surface phonon polaritons. *Nanophotonics* **4**, 44–68 (2015).
96. Zhang, L. et al. Correlated metals as transparent conductors. *Nat. Mater.* **15**, 204–210 (2016).
97. Wen, X. et al. Doubly enhanced second harmonic generation through structural and epsilon-near-zero resonances in TiN nanostructures. *ACS Photonics* **5**, 2087–2093 (2018).
98. Gu, L., Livenere, J., Zhu, G., Narimanov, E. E. & Noginov, M. A. Quest for organic plasmonics. *Appl. Phys. Lett.* **103**, 021104 (2013).
99. Woo, B. H. et al. Dispersion control of excitonic thin films for tailored superabsorption in the visible region. *ACS Photonics* **4**, 1138–1145 (2017).
100. Sachet, E. et al. Dysprosium-doped cadmium oxide as a gateway material for mid-infrared plasmonics. *Nat. Mater.* **14**, 414–420 (2015).
101. Spitzer, W. G., Kleinman, D. & Walsh, D. Infrared properties of hexagonal silicon carbide. *Phys. Rev.* **113**, 127–132 (1959).
102. Kim, J. et al. Role of epsilon-near-zero substrates in the optical response of plasmonic antennas. *Optica* **3**, 339–346 (2016).
103. Kischkat, J. et al. Mid-infrared optical properties of thin films of aluminum oxide, titanium dioxide, silicon dioxide, aluminum nitride, and silicon nitride. *Appl. Opt.* **51**, 6789–6798 (2012).
104. Shahsafi, A. et al. Mid-infrared optics using dielectrics with refractive indices below unity. *Phys. Rev. Appl.* **10**, 034019 (2018).
105. Ou, J.-Y. et al. Ultraviolet and visible range plasmonics in the topological insulator $Bi_{1.5}Sb_{0.5}Te_{1.8}Se_{1.2}$. *Nat. Commun.* **5**, 5139 (2014).
106. Braic, L. et al. Titanium oxynitride thin films with tunable double epsilon-near-zero behavior for nanophotonic applications. *ACS Appl. Mater. Interfaces* **9**, 29857–29862 (2017).
107. Pollard, R. J. et al. Optical nonlocalities and additional waves in epsilon-near-zero metamaterials. *Phys. Rev. Lett.* **102**, 127405 (2009).
108. Lepeshkin, N. N., Schweinsberg, A., Piredda, G., Bennink, R. S. & Boyd, R. W. Enhanced nonlinear optical response of one-dimensional metal–dielectric photonic crystals. *Phys. Rev. Lett.* **93**, 123902 (2004).
109. Subramania, G., Fischer, A. J. & Luk, T. S. Optical properties of metal–dielectric based epsilon near zero metamaterials. *Appl. Phys. Lett.* **101**, 241107 (2012).
110. Yang, X. et al. Experimental demonstration of near-infrared epsilon-near-zero multilayer metamaterial slabs. *Opt. Express* **21**, 23631–23639 (2013).
111. Maas, R., Parsons, J., Engheta, N. & Polman, A. Experimental realization of an epsilon-near-zero metamaterial at visible wavelengths. *Nat. Photonics* **7**, 907–912 (2013).
112. Cai, W. & Shalaev, V. *Optical Metamaterials* (Springer, 2010).
113. Poddubny, A., Iorsh, I., Belov, P. & Kivshar, Y. Hyperbolic metamaterials. *Nat. Photonics* **7**, 958–967 (2013).
114. Caligiuri, V., Palei, M., Imran, M., Manna, L. & Krahne, R. Planar double-epsilon-near-zero cavities for spontaneous emission and Purcell effect enhancement. *ACS Photonics* **5**, 2287–2294 (2018).
115. Pendry, J., Holden, A., Robbins, D. & Stewart, W. Magnetism from conductors and enhanced nonlinear phenomena. *IEEE Trans. Microw. Theory Tech.* **47**, 2075–2084 (1999).
116. Valentine, J. et al. Three-dimensional optical metamaterial with a negative refractive index. *Nature* **455**, 376–379 (2008).
117. Yun, S. et al. Low-loss impedance-matched optical metamaterials with zero-phase delay. *ACS Nano* **6**, 4475–4482 (2012).
118. Pendry, J., Brien, S. O. & Pendry, J. B. Photonic band-gap effects and magnetic activity in dielectric composites. *J. Phys. Condens. Matter* **14**, 4035–4044 (2002).
119. Holloway, C. L., Kuester, E. F., Baker-Jarvis, J. & Kabos, P. A double negative (DNG) composite medium composed of magnetodielectric spherical particles embedded in a matrix. *IEEE Trans. Antennas Propag.* **51**, 2596–2603 (2003).
120. Yang, Y. et al. Dielectric meta-reflectarray for broadband linear polarization conversion and optical vortex generation. *Nano Lett.* **14**, 1394–1399 (2014).
121. Khorasaninejad, M. et al. Metalenses at visible wavelengths: diffraction-limited focusing and subwavelength resolution imaging. *Science* **352**, 1190–1194 (2016).
122. Moitra, P. et al. Realization of an all-dielectric zero-index optical metamaterial. *Nat. Photonics* **7**, 791–795 (2013).
123. Huang, X., Lai, Y., Hang, Z. H., Zheng, H. & Chan, C. T. Dirac cones induced by accidental degeneracy in photonic crystals and zero-refractive-index materials. *Nat. Mater.* **10**, 582–586 (2011).
124. Vulis, D. I. et al. Monolithic CMOS-compatible zero-index metamaterials. *Opt. Express* **25**, 12381–12399 (2017).
125. Kita, S. et al. On-chip all-dielectric fabrication-tolerant zero-index metamaterials. *Opt. Express* **25**, 8326–8334 (2017).
126. Reshef, O. et al. Direct observation of phase-free propagation in a silicon waveguide. *ACS Photonics* **4**, 2385–2389 (2017).
127. Schulz, S. A. et al. Optical response of dipole antennas on an epsilon-near-zero substrate. *Phys. Rev. A* **93**, 063846 (2016).
128. Alam, M. Z., Schulz, S. A., Upham, J., De Leon, I. & Boyd, R. W. Large optical nonlinearity of nanoantennas coupled to an epsilon-near-zero material. *Nat. Photonics* **12**, 79–83 (2018).
129. Hendrickson, J. R. et al. Coupling of epsilon-near-zero mode to gap plasmon mode for flat-top wideband perfect light absorption. *ACS Photonics* **5**, 776–781 (2018).
130. Guo, P., Chang, R. P. & Schaller, R. D. Transient negative optical nonlinearity of indium oxide nanorod arrays in the full-visible range. *ACS Photonics* **4**, 1494–1500 (2017).
131. Taghinejad, M. et al. Ultrafast control of phase and polarization of light expedited by hot-electron transfer. *Nano Lett.* **18**, 5544–5551 (2018).
132. Howes, A., Wang, W., Kravchenko, I. & Valentine, J. Dynamic transmission control based on all-dielectric Huygens metasurfaces. *Optica* **5**, 787–792 (2018).
133. Liberal, I., Mahmoud, A. M., Li, Y., Edwards, B. & Engheta, N. Photonic doping of epsilon-near-zero media. *Science* **355**, 1058–1062 (2017).
134. Kern, C. et al. Comparison of femtosecond laser-induced damage on unstructured vs. nano-structured Au-targets. *Appl. Phys. A* **104**, 15–21 (2011).
135. Neira, A. D. et al. Eliminating material constraints for nonlinearity with plasmonic metamaterials. *Nat. Commun.* **6**, 7757 (2015).

136. Bennink, R. S., Yoon, Y.-K., Boyd, R. W. & Sipe, J. E. Accessing the optical nonlinearity of metals with metal–dielectric photonic bandgap structures. *Opt. Lett.* **24**, 1416–1418 (1999).
137. Ferrera, M. & Carnemolla, E. G. Ultra-fast transient plasmonics using transparent conductive oxides. *J. Opt.* **20**, 024007 (2018).
138. Benis, S., Hagan, D. J. & Van Stryland, E. W. Enhancement mechanism of nonlinear optical response of transparent conductive oxides at epsilon-near-zero. *Conference on Lasers and Electro-Optics*, FF2E.1 (OSA, 2018).
139. Ferdinandus, M. R., Hu, H., Reichert, M., Hagan, D. J. & Van Stryland, E. W. Beam deflection measurement of time and polarization resolved ultrafast nonlinear refraction. *Opt. Lett.* **38**, 3518–3521 (2013).
140. Ferdinandus, M. R., Reed, J. M., Averett, K. L., Hopkins, F. K. & Urbas, A. Analysis of beam deflection measurements in the presence of linear absorption. *Opt. Mater. Express* **7**, 1598–1605 (2017).
141. Vincenti, M. A., de Ceglia, D., Haus, J. W. & Scalora, M. Harmonic generation in multiresonant plasma films. *Phys. Rev. A* **88**, 043812 (2013).
142. Vincenti, M. A., de Ceglia, D., Angelis, C. D. & Scalora, M. Surface-plasmon excitation of second-harmonic light: emission and absorption. *J. Opt. Soc. Am. B* **34**, 633–641 (2017).
143. Scalora, M. et al. Harmonic generation from metal–oxide and metal–metal boundaries. *Phys. Rev. A* **98**, 023837 (2018).
144. de Ceglia, D., Vincenti, M. A., Akozbek, N., Bloemer, M. J. & Scalora, M. Nested plasmonic resonances: extraordinary enhancement of linear and nonlinear interactions. *Opt. Express* **25**, 3980–3990 (2017).
145. Sundgren, J. E., Johansson, B. O., Karlsson, S. E. & Hentzell, H. T. G. Mechanisms of reactive sputtering of titanium nitride I: influence of process parameters on film. *Thin Solid Films* **105**, 367–384 (1983).
146. Batzill, M. & Diebold, U. The surface and materials science of tin oxide. *Prog. Surf. Sci.* **79**, 47–154 (2005).
147. Kippenberg, T. J., Holzwarth, R. & Diddams, S. A. Microresonator-based optical frequency combs. *Science* **332**, 555–559 (2011).
148. Michaeli, L., Keren-Zur, S., Avayu, O., Suchowski, H. & Ellenbogen, T. Nonlinear surface lattice resonance in plasmonic nanoparticle arrays. *Phys. Rev. Lett.* **118**, 243904 (2017).
149. Hendrickson, J. R. et al. Plasmonic enhancement of epsilon-near-zero modes. *Advanced Photonics Congress* NpTh4C.2 (OSA, 2018).
150. Taghinejad, M. et al. Hot-electron-assisted femtosecond all-optical modulation in plasmonics. *Adv. Mater.* **30**, 1704915 (2018).
151. Kim, J. et al. Dynamic control of nano-cavities with tunable metal oxides. *Nano Lett.* **18**, 740–746 (2017).
152. Suchowski, H. et al. Phase mismatch-free nonlinear propagation in optical zero-index materials. *Science* **342**, 1223–1226 (2013).
153. Mattiucci, N., Bloemer, M. J. & D'Aguanno, G. Phase-matched second harmonic generation at the Dirac point of a 2-D photonic crystal. *Opt. Express* **22**, 6381–6390 (2014).
154. Reshef, O. et al. Phase-matching in Dirac-cone-based zero-index metamaterials. *CLEO: Applicatins and Technology*, jTu5A.53. (OSA, 2016).
155. Vincenti, M. A., de Ceglia, D. & Scalora, M. Nonlinear dynamics in low permittivity media: the impact of losses. *Opt. Express* **21**, 29949–29954 (2013).
156. Kim, K. H. Unity-order nonlinear optical index change in epsilon-near-zero composite materials of gain media and metal nanoparticles. *Ann. Phys.* **530**, 1700259 (2018).
157. Berini, P. & De Leon, I. Surface plasmon-polariton amplifiers and lasers. *Nat. Photonics* **6**, 16–24 (2012).
158. De Leon, I. & Berini, P. Amplification of long-range surface plasmons by a dipolar gain medium. *Nat. Photonics* **4**, 382–387 (2010).
159. Campione, S. & Capolino, F. Composite material made of plasmonic nanoshells with quantum dot cores: Loss-compensation and $\epsilon$-near-zero physical properties. *Nanotechnology* **23**, 235703 (2012).
160. Vincenti, M. A., Campione, S., De Ceglia, D., Capolino, F. & Scalora, M. Gain-assisted harmonic generation in near-zero permittivity metamaterials made of plasmonic nanoshells. *New J. Phys.* **14**, 103016 (2012).
161. Rizza, C., Ciattoni, A. & Palange, E. Two-peaked and flat-top perfect bright solitons in nonlinear metamaterials with epsilon near zero. *Phys. Rev. A* **83**, 053805 (2011).
162. Fleury, R. & Alù, A. Enhanced superradiance in epsilon-near-zero plasmonic channels. *Phys. Rev. B* **87**, 201101 (2013).
163. Prain, A., Vezzoli, S., Westerberg, N., Roger, T. & Faccio, D. Spontaneous photon production in time-dependent epsilon-near-zero materials. *Phys. Rev. Lett.* **118**, 133904 (2017).
164. Jahani, S., Zhao, H. & Jacob, Z. Switching Purcell effect with nonlinear epsilon-near-zero media. *Appl. Phys. Lett.* **113**, 021103 (2018).
165. Ciattoni, A., Marini, A. & Rizza, C. All-optical modulation in wavelength-sized epsilon-near-zero media. *Opt. Lett.* **41**, 3102–3105 (2016).
166. Neira, A., Wurtz, G. & Zayats, A. All-optical switching in Si photonic waveguides with epsilon-near-zero resonant cavity. *Photonics Res.* **6**, B1–B5 (2017).
167. Ciattoni, A., Rizza, C. & Palange, E. All-optical active plasmonic devices with memory and power-switching functionalities based on $\epsilon$-near-zero nonlinear metamaterials. *Phys. Rev. A* **83**, 43813 (2011).
168. Abdelatty, M. Y., Badr, M. M. & Swillam, M. A. High-speed hybrid plasmonic electro-optical absorption modulator exploiting epsilon-near-zero effect in indium-tin-oxide. *J. Nanophotonics* **12**, 036011 (2018).
169. Qiu, X., Ruan, X., Li, Y. & Zhang, F. Multi-layer MOS capacitor based polarization insensitive electro-optic intensity modulator. *Opt. Express* **26**, 13902–13914 (2018).
170. Sinatkas, G. & Kriezis, E. E. Silicon-photonic electro-optic phase modulators integrating transparent conducting oxides. *IEEE J. Quantum Electron.* **54**, 8400208 (2018).
171. Ricard, D., Roussignol, P. & Flytzanis, C. Surface-mediated enhancement of optical phase conjugation in metal colloids. *Opt. Lett.* **10**, 511–513 (1985).
172. Vogel, E. M., Weber, M. J. & Krol, D. Nonlinear optical phenomena in glass. *Phys. Chem. Glass.* **32**, 231–254 (1991).
173. Bloembergen, N., Burns, W. K. & Matsuoka, M. Reflected third harmonic generated by picosecond laser pulses. *Opt. Commun.* **1**, 195–198 (1969).
174. Smith, D. D. et al. z-scan measurement of the nonlinear absorption of a thin gold film. *J. Appl. Phys.* **86**, 6200–6205 (1999).
175. De Leon, I., Shi, Z., Liapis, A. C. & Boyd, R. W. Measurement of the complex nonlinear optical response of a surface plasmon-polariton. *Opt. Lett.* **39**, 2274–2277 (2014).
176. Ueda, N. et al. Third-order nonlinear optical susceptibilities of electroconductive oxide thin films. *Appl. Phys. Lett.* **59**, 502–503 (1991).
177. Sheik-Bahae, M., Said, A. A. & Van Stryland, E. W. High-sensitivity, single-beam $n_2$ measurements. *Opt. Lett.* **14**, 955–957 (1989).
178. Sheik-Bahae, M., Said, A., Wei, T.-H., Hagan, D. & Van Stryland, E. Sensitive measurement of optical nonlinearities using a single beam. *IEEE J. Quantum Electron.* **26**, 760–769 (1990).



**Acknowledgements**
The authors acknowledge support through the Natural Sciences and Engineering Research Council of Canada (NSERC), the Canada Research Chairs programme and the Canada First Research Excellence Fund. O.R. acknowledges the support of the Banting Postdoctoral Fellowship of the NSERC. I.D.L. acknowledges support from CONACyT (Ciencia Básica) grant no. 286150. R.W.B. also acknowledges support from the Defense Advanced Research Projects Agency (DARPA) Defense Sciences Office (DSO) Nascent programme and from the US Army Research Office.


**Author contributions**
O.R., I.D.L. and M.Z.A. researched data for the article. O.R., I.D.L., M.Z.A. and R.W.B. contributed to manuscript preparation, revision and editing.

**Competing interests**
The authors declare that they have no competing interests.

**Publisher's note**
Springer Nature remains neutral with regard to jurisdictional claims in published maps and institutional affiliations.